

THE OFFICIAL MAGAZINE OF THE OCEANOGRAPHY SOCIETY

Oceanography

CITATION

Clague, D.A., J.B. Paduan, D.W. Caress, W.W. Chadwick Jr., M. Le Saout, B.M. Dreyer, and R.A. Portner. 2017. High-resolution AUV mapping and targeted ROV observations of three historic lava flows at Axial Seamount. *Oceanography* 30(4):82–99, <https://doi.org/10.5670/oceanog.2017.426>.

DOI

<https://doi.org/10.5670/oceanog.2017.426>

COPYRIGHT

This article has been published in *Oceanography*, Volume 30, Number 4, a quarterly journal of The Oceanography Society. Copyright 2017 by The Oceanography Society. All rights reserved.

USAGE

Permission is granted to copy this article for use in teaching and research. Republication, systematic reproduction, or collective redistribution of any portion of this article by photocopy machine, reposting, or other means is permitted only with the approval of The Oceanography Society. Send all correspondence to: info@tos.org or The Oceanography Society, PO Box 1931, Rockville, MD 20849-1931, USA.



High-Resolution AUV Mapping and Targeted ROV Observations of Three Historical Lava Flows at Axial Seamount

By David A. Clague, Jennifer B. Paduan, David W. Caress, William W. Chadwick Jr.,
Morgane Le Saout, Brian M. Dreyer, and Ryan A. Portner

MBARI's autonomous underwater
vehicle. *Photo credit: Phil Sammet*

ABSTRACT. The lava flows produced by eruptions at Axial Seamount in 1998, 2011, and 2015 were mapped at 1 m resolution from autonomous underwater vehicles (AUVs) developed at the Monterey Bay Aquarium Research Institute (MBARI). A portion of the flows erupted in 2011 and 2015 are defined by pre- and post-eruption AUV surveys. Data processing software, also developed at MBARI, precisely coregisters pre- and post-eruption surveys to allow construction of difference maps by subtracting a pre-eruption grid from a post-eruption grid. Such difference maps are key to extracting detailed information about eruptive processes and emplacement of the lava flows. All three eruptions began on the east side of the caldera, and each produced $\sim 25 \times 10^6 \text{ m}^3$ of thin channelized flows (with sheet lava channels, lobate lava interiors with pillars, and distal inflated pillow lobes) in the caldera and on the upper south or north rifts. The 1998 and 2011 eruptions propagated down the south rift, and the 2015 eruption propagated down the north rift. The 2011 and 2015 eruptions formed shallow grabens surrounding new non-eruptive open fissures on the east rim of the caldera and produced thick hummocky flows on upper to mid rifts, and the 2011 eruption also produced a thick hummocky flow on the lower south rift. Future eruptions at Axial Seamount will likely follow this pattern, regardless of which rift is the locus of the eruption.

INTRODUCTION

The most voluminous volcanic activity on Earth occurs in the deep sea (Crisp, 1984) along the global 65,000 km-long mid-ocean ridge system. Despite the high frequency of submarine eruptions required to construct oceanic crust, these eruptions are rarely detected and even more rarely studied in detail to understand eruption processes and lava flow emplacement in the submarine realm (e.g., Fornari et al., 2012; Rubin et al., 2012). Historical submarine eruptions on mid-ocean ridges have been discovered by water-column surveys that detected large water masses with temperature and chemical anomalies (megaplumes) above eruption sites, during submersible dives that serendipitously encountered new glassy lava flows, by repeat bathymetry surveys that revealed depth changes of the seafloor, or by recording of seismic activity on hydrophone arrays that accompanied these explorations. Most recently, instruments on the Ocean Observatory Initiative (OOI) cabled undersea network (Kelley et al., 2014, 2015; Wilcock et al., 2016; Nooner and Chadwick, 2016)

detected a 2015 eruption in real time at Axial Seamount that triggered a rapid response cruise (Chadwick et al., 2016).

Axial Seamount is a submarine volcano astride the Juan de Fuca Ridge, 400 km offshore the US Pacific Northwest (Figure 1). It has a horseshoe-shaped 3×8 km summit caldera that is deepest to the northeast and whose rim is buried by lava flows to the southeast. The summit is connected to north- and south-trending rift zones (Figure 1) and rises to a depth of $\sim 1,367$ m with the shallowest area on the southwest rim. The three detected eruptions at Axial Seamount in 1998, 2011, and 2015 are the most recent of >50 mapped lava flows emplaced in the last 1,600 years (Clague et al., 2013).

High-resolution autonomous underwater vehicle (AUV) bathymetric mapping data of the historical flows on Axial Seamount have illuminated how effusive lava flows are emplaced under varying eruptive conditions and the dynamics of eruptive activity (Caress et al., 2012; Chadwick et al., 2013, 2016; Yeo et al., 2013). The mapping, combined with lava and sediment core sample collection

using remotely operated vehicles (ROVs), has enabled development of eruptive and tectonic histories of Axial Seamount and of the Endeavour Segment of the Juan de Fuca Ridge (Clague et al., 2013, 2014) that enhance study of recent volcanic and hydrothermal activity on mid-ocean ridges. High-resolution mapping has also illuminated the distribution of eruptive and non-eruptive fissures, and the relation of flow types and fissures to pre- and syn-eruptive geophysical observations. The mapping data also permit accurate calculation of flow volumes, but uncertainties in eruption duration still hamper determination of eruption rates. The scientific results made possible by these Monterey Bay Aquarium Research Institute (MBARI) technological advancements in high-resolution seafloor mapping are outlined here as part of this special issue celebrating MBARI's 30-year anniversary.

MAPPING AUV SURVEYS AT AXIAL SEAMOUNT

One of the primary tools for building understanding of submarine eruptive processes is the ability to map the lava flows and eruptive fissures at high resolution. Mapping of lava flows on the ridge system using images from ship-based sonars, towed side-scan sonars and cameras, and bottom observations from submersibles began in the late 1970s (e.g., Ballard and van Andel, 1977; Ballard et al., 1979). More recent observation and sampling studies have used ROVs that are spatially located using GPS-based long-baseline or ultra-short baseline navigation. AUV mapping technology and data processing techniques developed at MBARI have focused on sites of historical (since the mid-1980s) eruptions on the Juan de Fuca and Gorda Ridges offshore northwestern North America. Lava flows produced during these eruptions

were studied in considerable detail soon after their discovery (e.g., Fox et al., 1992; Embley et al., 1995, 1999, 2000; Chadwick and Embley, 1998; Chadwick et al., 1998) and provide context for high-resolution mapping data.

Between 2006 and 2016, MBARI mapping AUVs (Caress et al., 2008) collected 1 m lateral, 10 cm vertical resolution bathymetry and side-scan data on Axial Seamount during 37 surveys as part of six expeditions on four research ships. The MBARI surveys were augmented using Woods Hole Oceanographic Institution's (WHOI's) AUV *Sentry* for four surveys in 2015, and five in 2017. All 41 surveys completed by 2016 have been coregistered spatially by matching features in overlapping data and solving for

a single, comprehensive AUV navigation model. The surveys were conducted with AUV altitudes between 50 m and 90 m, with most at 50 m altitude. The current coverage at Axial encompasses 290 km², including significant areas resurveyed after the 2011 and 2015 eruptions to detect seafloor change.

The submarine volcanic process studies undertaken at Axial Seamount require well-navigated, repeatable, efficiently collected high-resolution seafloor mapping data at depths ranging from 1,400 m to over 2,500 m. Over the past 15 years, these science requirements have helped to drive continuing innovation in autonomous vehicle, sensor, and data processing technologies. MBARI began these surveys with a single mapping AUV

capable of eight-hour surveys covering 30 km of survey lines; by 2016, two AUVs were operated simultaneously with each achieving 17-hour survey durations for a total 160 km of surveying per day, along with a fivefold increase in bathymetric sounding density. Equally significant, the MB-System software package used for survey planning and data processing (Caress and Chayes, 1996, 2011; Caress et al., 2008) has evolved to solve the problems particular to surveying challenging submarine topography. The near-vertical walls of Axial caldera required automated pre-planning of the AUV vertical trajectory to avoid bottom crashes, and the high and narrow walls of some drained lava ponds require multistage missions combining sections of constant depth and constant altitude operation.

For any deep-ocean AUV-based seafloor survey, the primary data processing challenge is achieving navigational accuracy similar to the 1 m bathymetric lateral resolution. Although the inertial navigation system (INS) used on MBARI AUVs limits navigational errors to 0.05% of distance traveled, this translates to as much as 40 m accumulated error for an 80 km trackline survey. Coregistration within and between surveys at the 1 m level is attained by measuring both the lateral and the vertical navigational offsets required to match bathymetric features in crossing and overlapping swaths, and then solving for an optimal navigational model fitting those features while also satisfying known feature positions (e.g., vent chimney locations from ROV dives) and minimizing perturbations to vehicle speed. On Axial Seamount, the caldera floor uplifts slowly as the subsurface magma reservoir inflates and subsides rapidly during eruptions that drain the reservoir (Nooner and Chadwick, 2016). Consequently, bathymetric changes reflect both lava emplacement and vertical deformation associated with the eruption cycle. Because it measures horizontal and vertical navigation offsets required to match features, the MB-System navigation adjustment tool allows differencing

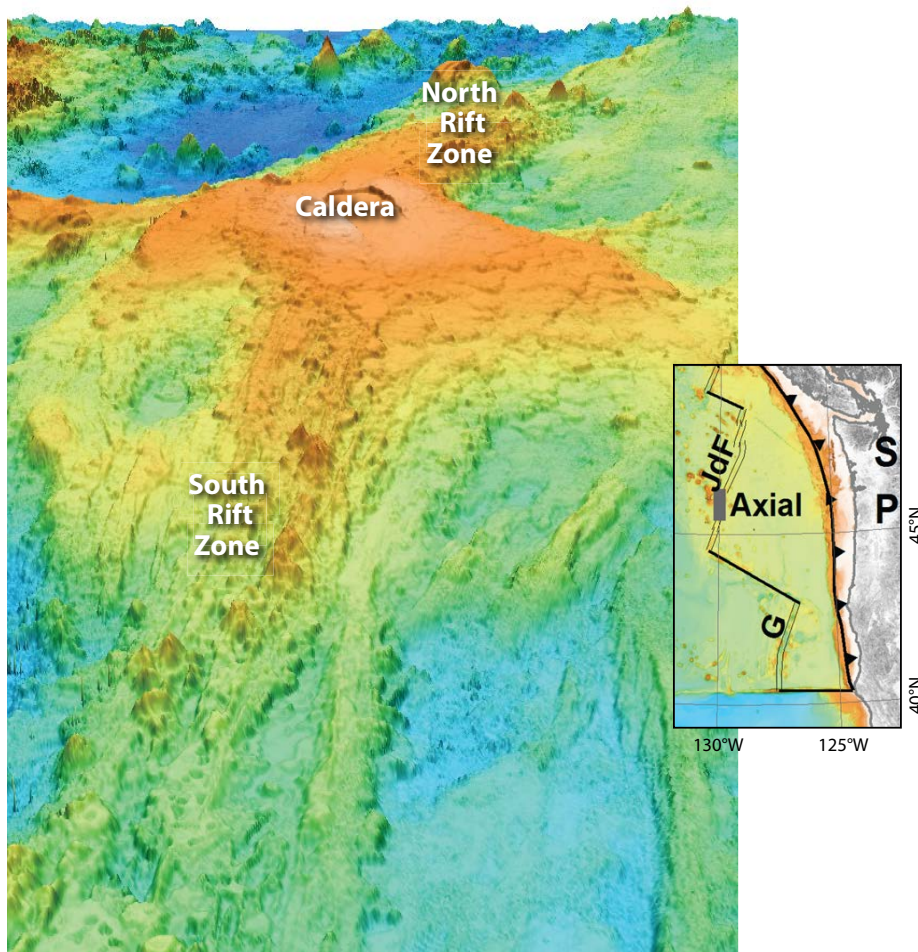


FIGURE 1. Oblique view of Axial Seamount. View is to the north and has 3x vertical exaggeration with the color ramp from 3,000 m to 1,300 m. The north and south rifts are labeled, as is the summit caldera. Inset shows location of Axial Seamount offshore Oregon and Washington. S is Seattle, P is Portland, G is Gorda Ridge, and JdF is Juan de Fuca Ridge. The gray box is the extent of the map in Figure 2a.

repeated and coregistered AUV bathymetry surveys to quantitatively measure both types of seafloor change.

These advances in data collection and processing have allowed us to successfully address increasingly ambitious scientific questions at Axial Seamount. The historic flows have now been completely mapped at high resolution (Caress et al., 2012; Chadwick et al., 2013, 2016), and a geological and petrological history of the caldera floor, rim, and upper south rift has been developed (Clague et al., 2013; Dreyer et al., 2013). The many flows defined in the mapping data, when combined with radiocarbon ages of the base

of sediment cores on the flows, show that Axial Seamount has erupted >50 times in the past 1,600 years. The backscatter mapping data define regions around the summit where volcanoclastic sediments blanket the surface and provide a guide to sampling of those deposits (Helo et al., 2011; Portner et al., 2015).

Difference maps of 1 m resolution pre- and immediately post-2011 eruption AUV surveys (Caress et al., 2012) precisely defined, for first time, new submarine lava flows and their volumes even where they are only about 20 cm thick. Similar difference maps defined lava flows erupted in 2015 (Chadwick et al.,

2016). Where flows covered ground that had only been mapped at low resolution before the eruptions, calculations were imprecise, but the post-eruption high-resolution maps revealed important details obscured in lower-resolution post-eruption ship-based data. The repeat surveys used to define the extent of new flows can also be used to measure vertical deformation associated with subsurface magma accumulation between eruptions and discharge during eruptions (Caress et al., 2015, 2016). The summit and the neo-volcanic axes of the north and south rift zones are now mapped at high resolution (Figure 2). The hope is that

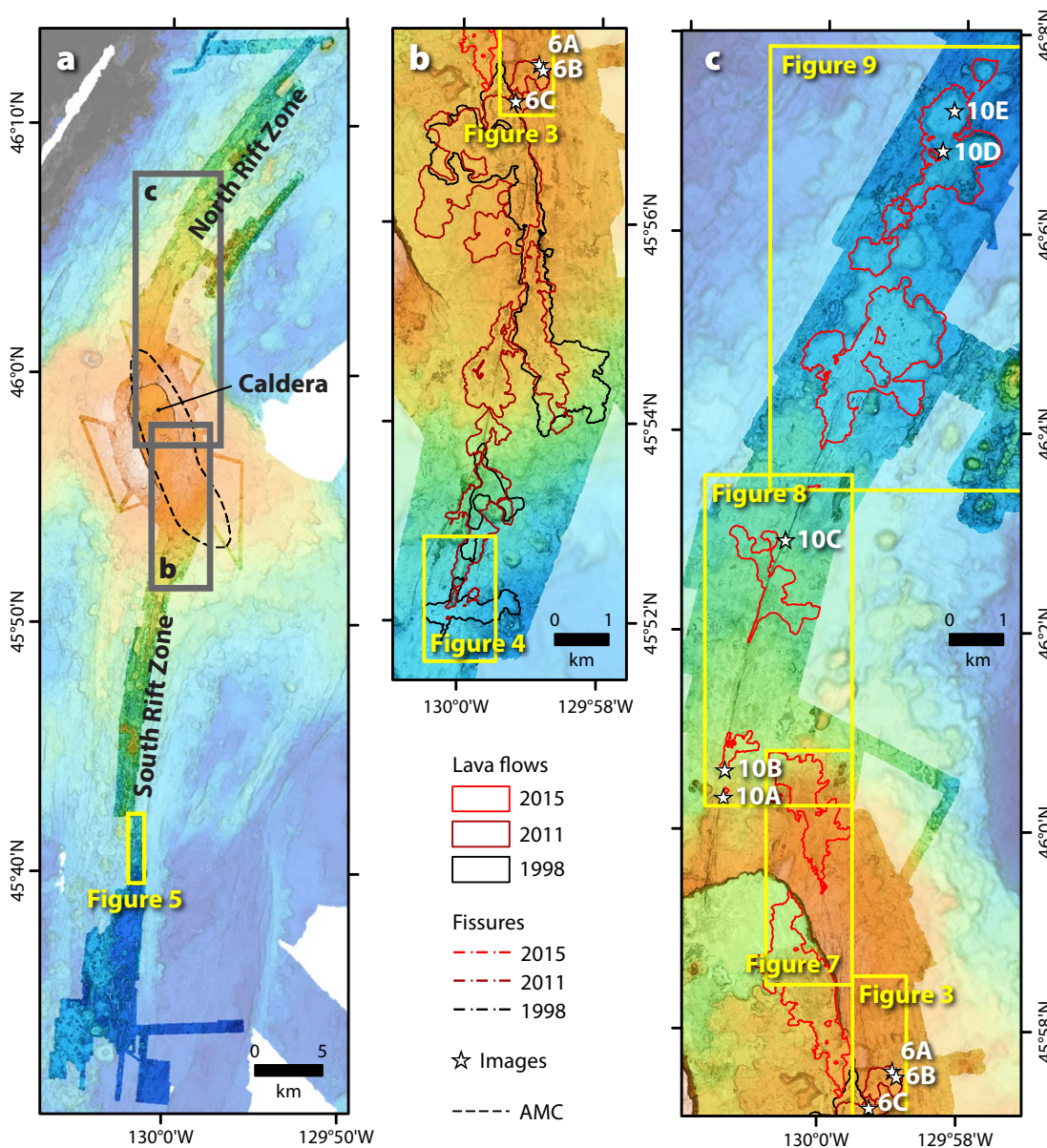


FIGURE 2. (a) Axial Seamount ship bathymetry (faded) underlying autonomous underwater vehicle (AUV) 1 m resolution coverage. The shape of the axial magma chamber (AMC) is indicated by the black dashed line, from Arnulf et al. (2014). Gray boxes in (a) show extents of panels (b) and (c), which are at the same scale, and yellow boxes on (a)–(c) show extents of subsequent map figures. Color ramp is from 2,550–1,375 m depth (blue to orange). (b) The flows of 1998 (Chadwick et al., 2013) and 2011 (modified from Caress et al., 2012). Color ramp is 2,300–1,390 m depth (blue to orange). (c) The 2015 flows in the summit caldera, on the northeast rim, and in the north rift zone (modified from Chadwick et al., 2016). Flow outlines (solid lines) and fissures (dotted lines) on subsequent maps use the same colors. Labeled stars indicate locations of images in Figures 6 and 10.

future eruptions at Axial Seamount will occur where high-resolution bathymetry now exists.

The lava flows erupted in 1998 were mapped in their entirety after the eruption as described in Chadwick et al. (2013), so we will briefly summarize their

1999; Chadwick et al., 2013). A difference map, subtracting the pre-eruption grid from the post-eruption grid, only clearly detected the distal pillow lobes, as the rest of the flows were too thin. The co-eruption earthquake swarm recorded by the SOSUS hydrophones continued

margins, lobate and drained flow interiors (with lava pillars), and the full range of sheet flow morphologies in channels. All are considered to be facies within map-scale channelized flows.

The 1998 eruption produced four channelized flows from 11 en echelon discontinuous fissures spread over 11 km (Chadwick et al., 2013). The distal southernmost lava flow consisted of a shingled sequence of distal pillow lobes up to 26 m thick where it flowed down a moderate slope east of the south rift. The northernmost flow also evolved into pillow lobes up to 13 m thick at the ends of channelized flows that had well-developed proximal sheet lava channels. Chadwick et al. (2013) estimated that the eruption produced $\sim 31 \times 10^6 \text{ m}^3$ of lava, although this volume is less precise than estimates for the 2011 or 2015 eruptions because the pre-eruption surface is defined from much lower-resolution ship-based bathymetry, and the flows are generally thin, so small errors in thickness result in large errors in volume. They also proposed that the eruption of the northern flow lasted < 12 hours based on the 2.5-hour rise and fall of an instrument package containing a pressure gauge that was partly engulfed by the flow (Fox et al., 2001), and that the channelized flows were consistent with high eruption rates. The minimum 2.5 and maximum 12 hour durations require average eruption rates from 2,400 to $500 \text{ m}^3 \text{ s}^{-1}$, with the lower rate thought to be more likely than the higher one.

New Results

New AUV mapping of much of the south rift (Figure 2a) and comparison to pre-1998 ship bathymetry did not detect any 1998 lava flows there, in agreement with earlier results based on pre- and post-eruption ship surveys. Revised volumes of the channelized flows erupted in the caldera and upper south rift were calculated at $24.1 \pm 1.5 \times 10^6 \text{ m}^3$ based on the area of the flows and new measurements of average thickness of the similar channelized flows erupted in 2011 and 2015 (discussed below, Table 1). This volume is

“For any deep-ocean AUV-based seafloor survey, the primary data processing challenge is achieving navigational accuracy similar to the 1 m bathymetric lateral resolution.”

results and add some new observations. The 2011 lava flows were mainly emplaced where pre-eruption mapping had been completed. The post-eruption and difference maps for those flows not yet mapped when Caress et al. (2012) was published are presented here. Finally, the 2015 lava flows were also only partly mapped before and immediately after the eruption (Chadwick et al., 2016). Previously unmapped 2015 flows are presented here.

1998 ERUPTION

Background

The eruption in 1998 was detected by the US Navy's SOSUS acoustic array (Dziak and Fox, 1999), and additional data were recovered after the eruption from instruments deployed as part of the National Oceanic and Atmospheric Administration (NOAA) NeMO observatory (Baker et al., 1999; Fox, 1999; Fox et al., 2001). The eruption began on January 25, and the swarm of earthquakes lasted for 11 days (Dziak and Fox, 1999). Pre-eruption ship multibeam and side-scan data (Embley et al., 1990) were compared with post-eruption ship-based surveys (Embley et al., 1999) and time-series observations (Embley et al.,

~50 km down the south rift (Dziak and Fox, 1999), but comparison of pre- and post-eruption ship-based bathymetric surveys did not detect new lava flows in those distal areas (Chadwick et al., 2013). The post-eruption high-resolution AUV mapping of the summit and proximal south rift (Figure 2b), begun in 2006, resulted in a detailed flow outline and also revealed details of flow morphology (Chadwick et al., 2013).

Chadwick et al. (2013) introduced the concept of map-scale flow morphology, describing features that are on the scale of hundreds of meters, based largely on high-resolution mapping of the 1998 Axial Seamount flows using the MBARI AUV. They proposed the terminology that “inflated lobate flows” proximal to the eruptive fissure transition to distal “inflated pillow flows” as the flow progresses downslope away from the fissure. Here, we simplify their terminology to *channelized flows* that combine the facies of inflated lobate flows and inflated pillow flows. Soule et al. (2005) used this term to describe similar features on the East Pacific Rise. The map-scale channelized flows are composed of visual-scale lava morphologies, including pillowed

22% smaller than the $31 \times 10^6 \text{ m}^3$ calculated by Chadwick et al. (2013) using the same flow area.

ROV dives done in support of constructing the geological history of the summit of Axial Seamount (Clague et al., 2013) observed rare fragmented pillow lava in the caldera near a low-temperature hydrothermal vent area at the northern end of the 1998 fissures.

2011 ERUPTION

Background

During the 2011 eruption, the SOSUS array was not operational, and the event was discovered serendipitously during ROV dives to refurbish monitoring instruments deployed at the summit. Bottom pressure recorders, hydrophones, and other instruments that were recovered after the eruption (those not entombed in lava) yielded important information about the sequence of events. The 2011 eruption began on April 6 and lasted ~6 days, based on when the summit co-eruption deflation ended (Chadwick et al., 2012). Caress et al. (2012) presented a comparison of pre- and post-2011 AUV bathymetry and used difference maps to determine the extent, thicknesses, and volume of the summit and upper south rift flows. Caress et al. (2012) showed that many pre-existing lava channels were

reused by 2011 flows and that the 2011 eruption largely reused fissures active in 1998 or during prehistoric eruptions. This level of mimicry of both fissures and channel systems was a new insight into understanding eruption and emplacement of channelized flows.

Another map-scale flow morphology described by Chadwick et al. (2013) was “pillow mounds” (e.g., Yeo et al., 2013). This morphology was originally detected in historic flows by comparing pre- and post-eruption ship bathymetric data for nearby Juan de Fuca Ridge historic eruptions, including the 1986 North Cleft (Chadwick et al., 1991; Fox et al., 1992) and the 1982–1991 and 1993 CoAxial (Chadwick et al., 2001), and occurs among the Axial 2011 and 2015 flows. Here, we modify the terminology to *hummocky flows* that are mostly pillow lavas that form mounds or coalesced mounds or ridges on or close to eruptive fissures. In contrast to the “pillow mounds” proposed and illustrated by Chadwick et al. (2013) that lack molten cores, hummocky flows have small (dike-scale dimension) to voluminous molten cores. White et al. (2000) previously suggested that basaltic lava domes (pillow mounds) grew endogenously, and therefore had molten cores. The molten cores of nearly all these types of flows are evident from summit

collapses, levee-bounded lava ponds, surface tumuli, and off-fissure hummocky flows fed through tubes.

New Results

Mapping data collected in 2014 and presented here shed additional light on the emplacement of hummocky flows and the dynamics of the 2011 eruption. It produced dominantly channelized flows in the caldera and on the upper south rift. In contrast, the most distal flows on the upper south rift are hummocky flows, and the most distal flow on the lower south rift is a thick, steep-sided hummocky flow.

The post-eruption AUV maps allow us to recalculate the areas and volumes (Table 1) presented in Caress (2012). The revised volume is $94.0 \times 10^6 \text{ m}^3$ ($\sim 5 \times 10^6 \text{ m}^3$ less than the prior estimate). The volume of the channelized flows in the caldera and on the upper south rift is $28.7 \times 10^6 \text{ m}^3$. However, in addition to the channelized flows, the 2011 eruption also formed hummocky flows on the upper south rift with a volume of $5.1 \times 10^6 \text{ m}^3$, and hummocky flows on the lower south rift with a volume of $60.1 \times 10^6 \text{ m}^3$ ($\sim 5.9 \times 10^6 \text{ m}^3$ less than the prior estimated). These revised volumes are based on core-registered pre- and post-eruption AUV surveys, except for the lower rift hummocky flow and a

TABLE 1. Historical Lava Flows on Axial Seamount

| | Flows and Fissures | Fissure Length (km) | Area ($\times 10^6 \text{ m}^2$) | Maximum Flow Thickness (m) | Average Flow Thickness (m) | Volume ($\times 10^6 \text{ m}^3$) | Volume/km of Fissure ($\times 10^6 \text{ m}^3/\text{km}$) |
|------|---|---------------------|------------------------------------|----------------------------|----------------------------|--------------------------------------|--|
| 1998 | Channelized Flows | 8.0 | 7.14 | SR26 | 3.4* | 24.1 | 3.0 |
| | Eruptive and Non-Eruptive Fissures | 11.0 | 7.14 | 26 | 3.4* | 24.1 | 2.2 |
| 2011 | Channelized Flows | 8.1 | 8.20 | C16 | 3.2 | 28.7 | 3.5 |
| | Upper South Rift Hummocky Flows | 1.5 | 0.37 | SR29 | 22.6 | 5.1 | 3.4 |
| | Lower South Rift Hummocky Flows | 4.8 | 1.65 | SR167 | 36.4 | 60.1 | 12.5 |
| | Eruptive and Non-Eruptive Fissures | 35.0 | 10.23 | 167 | 9.2 | 94.0 | 2.7 |
| 2015 | Channelized Flows | 7.3 | 6.92 | NR24, C12 | 3.6 | 24.7 | 3.4 |
| | North Rift Hummocky Flows | 4.4 | 4.59 | NR126 | 28.0 | 130.5 | 29.7 |
| | Eruptive and Non-Eruptive Fissures | 20.0 | 11.51 | 126 | 13.5 | 155.2 | 7.8 |

*Average of channelized flow from 2011 and 2015
SR = South Rift; NR = North Rift; C = Caldera

small portion of the near-caldera channelized flows for which there are no pre-eruption AUV data. For these areas, ship-collected multibeam bathymetry (MBARI Mapping Team, 2001) was used for the pre-eruption map. The surface area covered by the flows increased slightly from $10.10 \times 10^6 \text{ m}^2$ to $10.23 \times 10^6 \text{ m}^2$.

New post-2011 eruption mapping shows channelized flows on the east rim of the caldera (Figure 3), hummocky flows just south of the channelized flows on the upper south rift (Figure 4), and a lower south rift thick hummocky flow (Figure 5). Two lava flows on the east rim of the caldera erupted from a new fissure (Figure 3) offset 160–220 m east from 1998 eruptive fissures on the caldera floor (Chadwick et al., 2013). The fissure did not cut through a pre-existing

500 m diameter prehistoric hummocky flow composed of pillow lava that is bisected by the caldera-bounding fault. It does, however continue at N12W for at least 1.3 km (Figure 3c) as a discontinuous, open, non-eruptive fissure within a several-meter-deep and roughly 20 m wide graben (Figure 3d). The flows on the east caldera rim have common fragmented lava lobes (Figure 6a) and covered volcanoclastic sediment (Portner et al., 2015) up to several meters thick (Figure 6b). The southern of the two flows cascaded over the 10 m tall caldera-bounding fault (Figure 6c).

Hummocky flows that erupted in 2011 covered 1998 channelized flows and also filled a gap between 1998 flows where only a non-eruptive fissure was observed in the pre-2011 bathymetry (F1 on

Figure 4a). Mounds on the upper south rift coalesced to form a smooth hummocky flow (HF on Figure 4b) up to 27 m thick with a volume of $4.8 \times 10^6 \text{ m}^3$. The northern portion of HF is inferred to be located on top of its eruptive fissure, and the upper surface is thought to have collapsed as its molten lava drained out.

A series of three small coalesced flows and one isolated steep hummocky flow just downrift of HF are up to 29 m thick. These upper south rift hummocky flows (combined volume $5.1 \times 10^6 \text{ m}^3$) all erupted along $\sim 1.7 \text{ km}$ of the same fissure that fed 1998 flows (Figure 4a,b). One small offset hummocky flow (OHF on Figure 4b) grew west of the fissure that erupted a series of small mounds and the lava that flowed down a channel in the underlying 1998 channelized flow, then

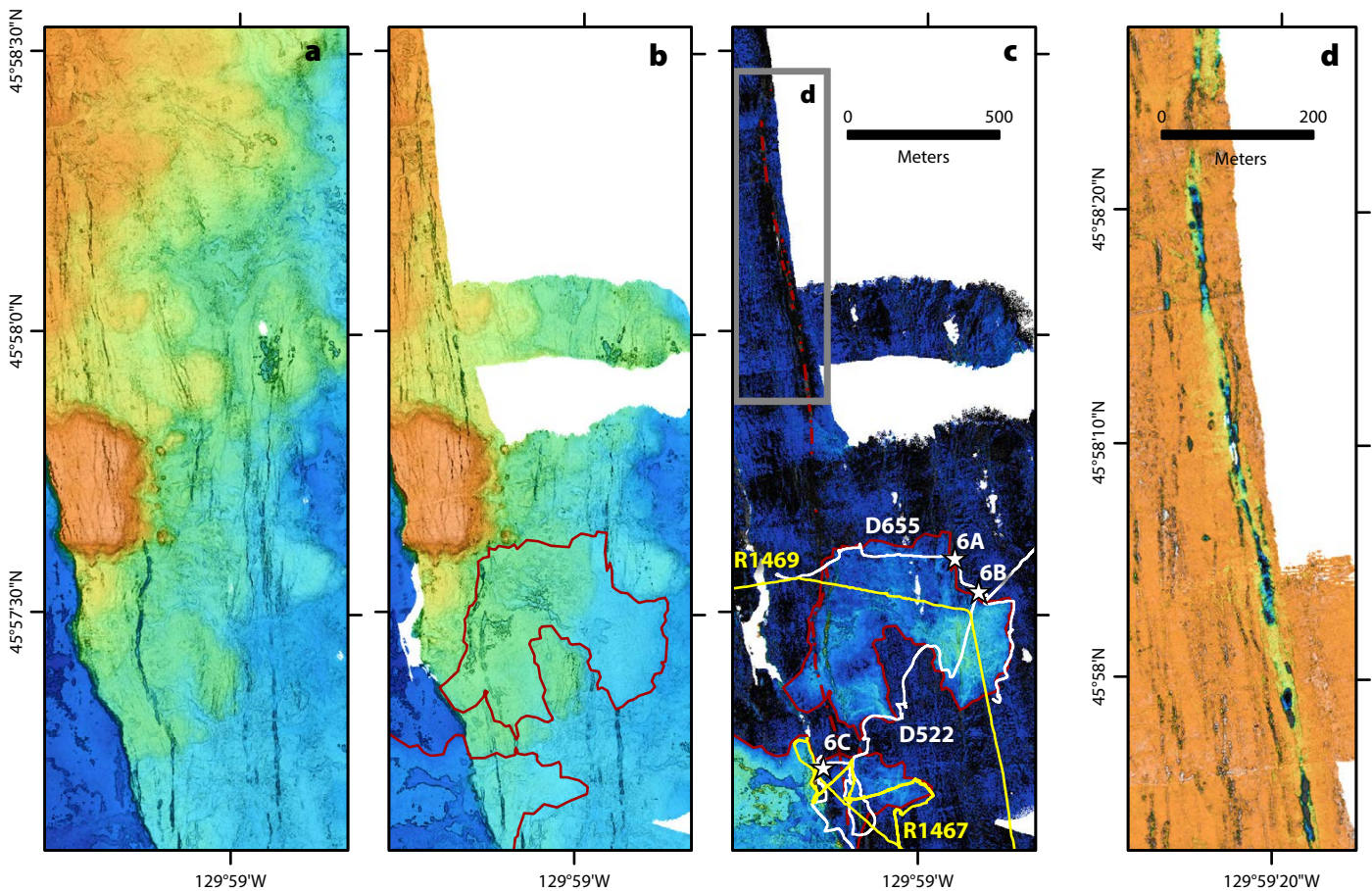


FIGURE 3. Maps showing the 2011 flows, fissure, and graben on the east rim of the caldera. (a) Pre-eruption AUV bathymetry, (b) post-eruption AUV bathymetry, and (c) and (d) difference maps from AUV bathymetry. Stars in (c) indicate locations of bottom photographs in Figure 6. (d) Close-up of the graben formed during the emplacement of the dike that also produced the discontinuous open fissure. Color ramps in (a) and (b) are 1,530–1,460 m depth (blue to orange), in (c) 0–15 m thickness (blue to orange), and in (d) (–4)–1 m thickness (blue to orange). (a, b, c) are at the same scale, and the location of (d) is the gray box in (c). ROV *Doc Ricketts* dives D522 and D655 are indicated by white lines, and ROV *ROPOS* dives R1467 and R1469 are tracked by yellow lines. Flow outlines in (b) and (c) and fissures in (c) as in key to Figure 1.

stalled, and then built upward. This displacement from the fissure demonstrates that even the smallest of hummocky flows had molten cores capable of feeding lateral flow.

The difference map (Figure 4c) also shows another fissure (F2) located about 300 m east of the main 1998/2011 eruptive fissure (F1 on Figure 4a). This 1.7 km long fissure overlaps the 1998/2011 fissure for about 1 km. One thin channelized flow 300 m across and one tiny low hummocky flow erupted from it.

These two parallel and overlapping fissures formed just 13 years after the south rift accommodated a dike that fed the 1998 eruption (F1 in Figure 4a, which was reused in 2011, and F2 in Figure 4c). The eruptive sections of the fissures overlap by about 650 m and non-eruptive

sections overlap by about 1 km. In 13 years, the average spreading rate on the Juan de Fuca Ridge should produce only 70 cm of extension, which is less than the space needed to accommodate a typical 1 m dike. Similar overlap of fissures took place during the 2015 eruption (discussed below), with eruptive and non-eruptive fissures on the northeast rim and the north rift overlapping by several hundred meters.

A different type of overlap between fissures occurs from one eruption to the next. The 2011 non-eruptive fissure on the east rim (Figure 3d) and the 2015 eruptive fissures on the caldera floor (Chadwick et al., 2016) overlap for nearly 1 km. In the intervening four years, spreading should have created only slightly more than 20 cm of extension, which is far less than

the width of a typical dike.

These observations suggest that extension at the summit of Axial during the last 20 years is significantly greater than simply the spreading rate multiplied by the time elapsed, and that spreading is either strongly episodic and each dike intrusion does not relieve all the accumulated tensional stress due to plate spreading, that the unbuttressed caldera walls allow inward collapse (as seen on the northwest rim), or that the flanks of the volcano are gravitationally sliding down and out, as occurs on larger volcanoes like Hawaii (e.g., Moore et al., 1989). Exploration of these options is beyond the scope of this paper.

The tall ridge consisting of coalesced steep hummocky flows on the lower south rift (Figure 5) is cryptic in the

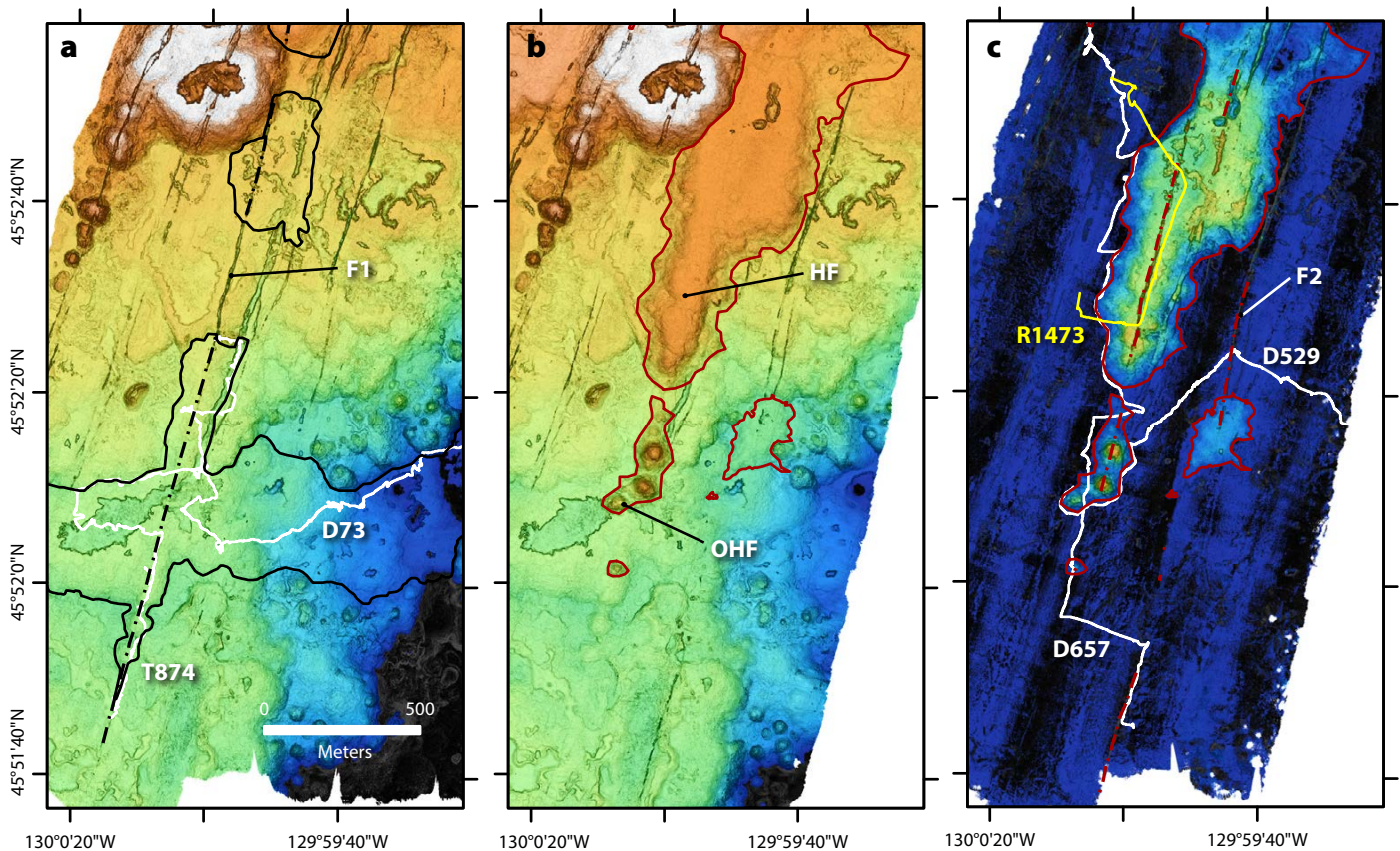


FIGURE 4. Upper south rift pillow ridge and new flows and fissures from 2011. (a) Pre-eruption AUV bathymetry with 1998 flow boundaries and fissure in black, and ROV *Tiburon* Dive T874 and ROV *Doc Ricketts* Dive D73 in white. (b) Post-eruption AUV bathymetry and (c) difference maps from AUV bathymetry. Color ramps in (a) and (b) are 1,775–1,660 m depth (blue to orange), and in (c) 0–41 m thickness (blue to orange). Post-2011 eruption ROV *Doc Ricketts* dives D529 and D657 are indicated by white lines, and the yellow line tracks ROV ROPOS Dive R1473. Flow outlines as in Figure 1, and fissures for each eruption are shown as dashed lines of the same color as the flows. Maps are uniform scale.

ship-based bathymetry, but evident on the difference map and has sharp contacts with underlying older flows (Figure 6). It erupted from a 4.8 km long fissure separated from the upper south rift hummocky flows by 18.2 km with no detected intervening surface fissure. The flow (Figure 5) lacks collapse structures. These hummocky flows align closely with a linear inferred eruptive fissure that is now buried by the flows. However, the feeding dike must have extended upward as the

mound grew, so at least a small part of the interior of the mound was molten. These steep hummocky flows were discharging low-temperature shimmering fluids (Figure 6f) 28 months after the eruption.

Pillows cascade down the steep slopes of the hummocky flows, forming talus slopes of pillow fragments at their bases. In places, the slopes are near vertical, and lava dripped off the tops of the mounds to form cylinder-like fragments (“lavacicles”) that accumulate at the base

of the slope (Figure 6e). Such lavacicles were previously observed among talus at the base of steep 1996 North Gorda Ridge hummocky flows (Clague et al., 2005; Yeo et al., 2013). The lavacicles demonstrate that the near-vertical slopes on some pillow mounds formed while the mound was still active and that the talus at the base also formed during the eruption. Talus deposits are generally viewed as being produced by tectonism subsequent to lava flow emplacement, but along mid-ocean ridges where many hummocky flows are steep because of very low eruption rates, talus and associated lavacicles are part of their construction during active eruptions (Paduan et al., 2014).

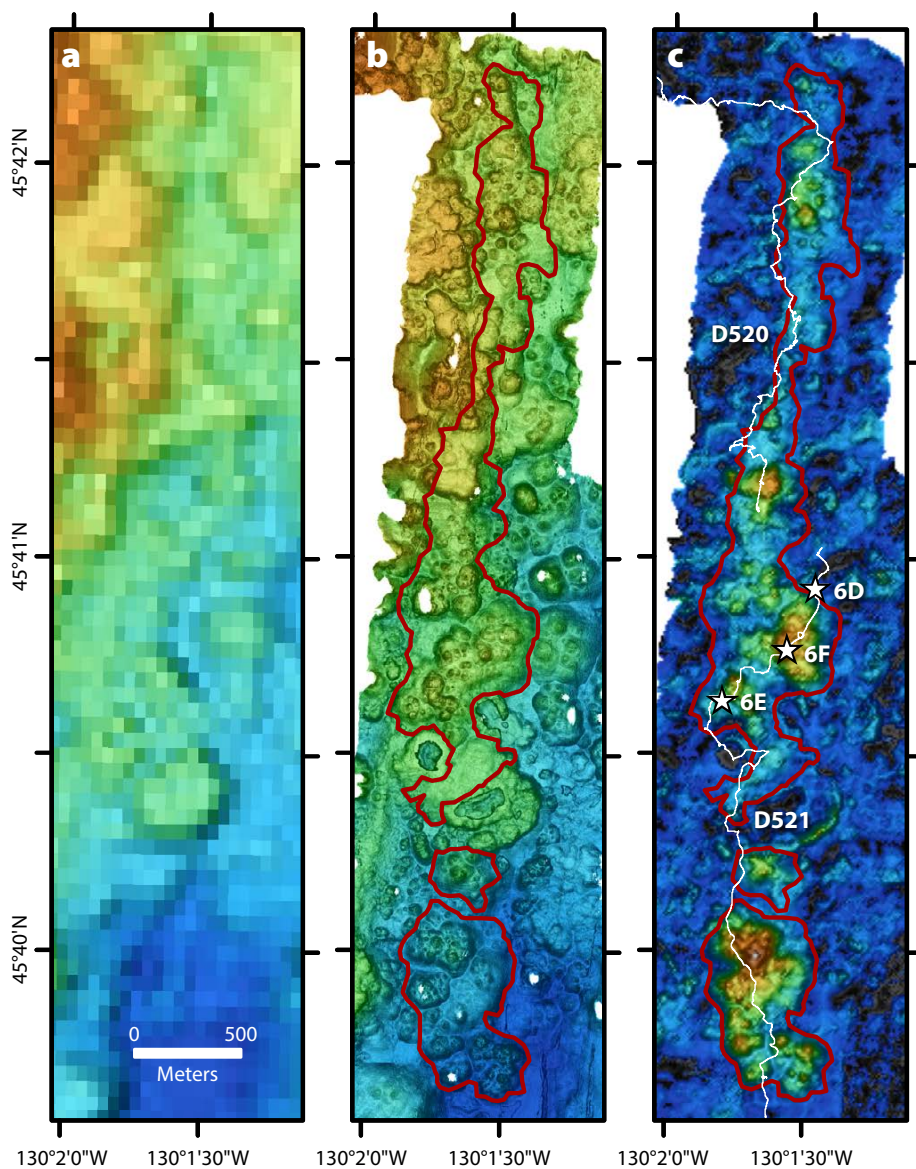


FIGURE 5. Lower south rift pillow mounds emplaced in 2011 are imaged by (a) pre-eruption ship bathymetry (MBARI Mapping Team, 2001) at 20 m resolution, (b) post-eruption AUV bathymetry at 1 m resolution, and (c) a difference map at 20 m resolution. Color ramps in (a) and (b) are 2,350–1,800 m depth (blue to orange), and in (c) is 0–158 m thickness (blue to orange). ROV *Doc Ricketts* dive D520 and D521 tracks are shown by white lines, and stars indicate locations of Figure 6 bottom photographs. Flow outlines as in Figure 1. The eruptive fissure is assumed to underlie the new pillow ridges and mound. Maps are uniform scale.

2015 ERUPTION Background

In 2015, the OOI cabled network was deployed at the summit of Axial Seamount but not yet fully operational. However, seismic and deformation (pressure and tilt) data were being sent via cable to shore, allowing detection of the eruption in real time (Wilcock et al., 2016; Nooner and Chadwick, 2016). The eruption began on April 24 and is inferred to have continued through May 21, when the last explosive sound was recorded from the north rift (Wilcock et al., 2016; Caplan-Auerbach et al., 2017). The 2015 lava flows are all located north of those erupted in 1998 and 2011 and have a more complex system of eruptive fissures (Figure 2c).

Difference maps based on pre- and post-eruption ship-based bathymetry broadly defined the thicker new hummocky flows on the north rift, and difference maps of pre-eruption AUV data and post-eruption ship data enabled higher-resolution AUV mapping of the thinner new channelized flows on the caldera floor and northeast of the caldera within a few months of the eruption (Chadwick et al., 2016). The eruptive fissures and flows within the caldera are described in detail in Chadwick et al. (2016), and our mapping of that area is the same with some additional coverage north-northeast of the caldera.

New Results

New AUV surveys and ROV *Doc Ricketts* dives in 2016 mapped the flows that remained unmapped in 2015. The mapping reveals several additional thin channelized flows (<1–2 m) not resolved by Chadwick et al. (2016) and shows that several north rift hummocky flows are not coalesced, as they had indicated. The post-eruptive AUV maps of the northeast caldera rim (Figure 7), the upper north rift (Figure 8), and the middle north rift (Figure 9) are

presented here. The 13 separate flows cover $11.51 \times 10^6 \text{ m}^2$ and have a combined volume of $155.2 \times 10^6 \text{ m}^3$ (Table 1, updated from Chadwick et al., 2016).

The flows north-northeast of the caldera (Figure 7) are thin channelized flows (no thicker than a few meters) with well-developed channels proximal to the eruptive fissures. Most of the largest flow on the north-northeast rim erupted from a fissure located between $45^\circ 59' 30'' \text{N}$ and 46°N (F1 in Figure 7c). The remainder of this flow erupted from

an en echelon west-stepping fissure near $46^\circ 10' \text{N}$, $130^\circ 20' \text{W}$ (F2 in Figure 7c).

The only other eruptive fissure north of the caldera, also an en echelon west-stepping, erupted two small flows (F3 in Figure 7c). This fissure is parallel to several prominent prehistoric fissures between the new flows and the caldera rim and on the upper north rift. Its N16E orientation is rotated 32° from the N16W orientation of the new F1 north-northeast of the caldera.

From the north-northeast caldera

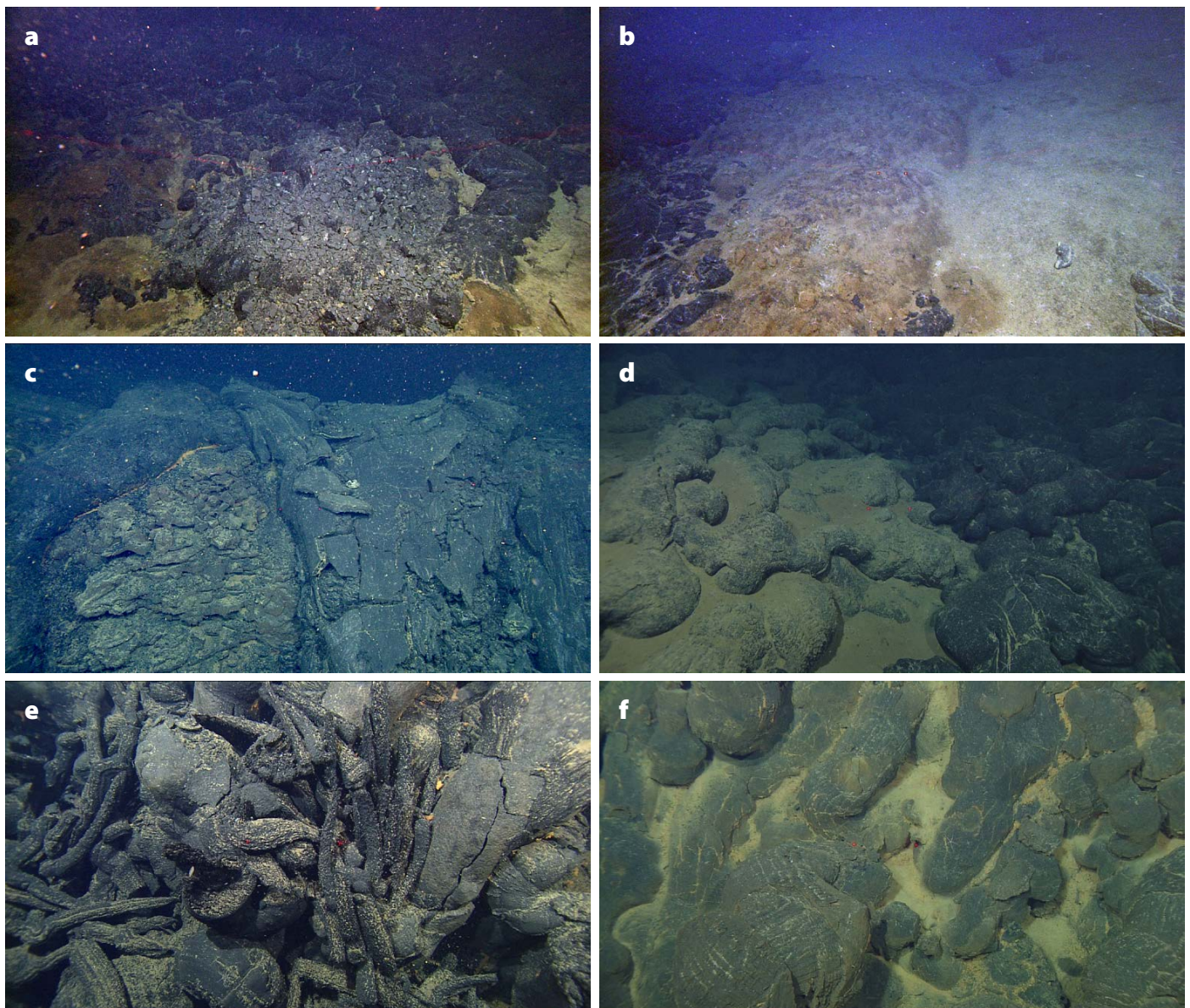


FIGURE 6. Plate of 2011-flow bottom photos with locations indicated on Figures 1b, 2c, and 4c. (a) The 2011 flow on the east rim showing explosion pits near the flow margin and dark sediment disrupted by flow burrowing under sediment. (b) Disrupted zone of sediment where flow has burrowed within >1 m of the sediment section. (c) Lava cascade on 10 m tall eastern caldera wall, with truncated old horizontal flows exposed behind the lava drapery. (d) The contact of the 2011 flow on top of an older flow on the lower south rift. (e) Lower south rift pillow ridge with lavacicles. (f) Hydrothermal deposits, and active venting on lower south rift pillow mounds.

rim, the eruptive fissures step westward ~1.2 km to N14E and align with the north rift. Here, two small, channelized flows erupted between 1.8 km and 2.6 km from the caldera. The southern flow has a 20 m diameter shatter ring probably formed above a lava tube as observed on land (Orr, 2011). The northern of the two flows on the upper north rift produced a drained lava pond with spindly pillars and arched flow top with thin crust (Figure 10b).

One of the most striking features revealed by the post-eruption mapping (Figure 7b) is a 1.7 km long, discontinuous, open, non-eruptive fissure embedded in a shallow graben between the northern-most eruptive fissure on the caldera floor and fissure F1 on the northeast caldera rim. The graben (Figure 7d)

is similar in depth (3–5 m) but twice as wide (~40 m) as that formed on the caldera rim during the 2011 eruption (Figure 3d). Its southern end is at about the same latitude as the northern end of the 2011 graben, but 400 m to the west.

Non-eruptive fissures and grabens form above dikes that did not reach the surface locally. The 2015 graben and fissure (Figure 7d) can be tied to geophysical data about the eruption. Seismic data indicate that the dike first propagated south from about 45°59'N to about 45°57'N before stalling and then migrating to the north (Wilcock et al., 2016). The initial rise of magma was therefore centered under the east rim of the caldera, within the zone where the non-eruptive fissure and graben (Figure 7) are located. The width and depth of the graben can

be used to estimate the width and depth below the surface of the dike that formed beneath it (Chadwick and Embley, 1998) and are consistent with a 0.8–2.1 m wide dike that rose to within 3 m of the surface at the north end, and 27 m at south end. The open fissures within the graben are discontinuous and up to at least 10 m deep. The initial southward migration of earthquakes extended south beyond the extent of the eruptive fissures on the caldera floor (Wilcock et al., 2016). The 2011 non-eruptive fissure and graben (Figure 3d) is narrower but similar in depth to those formed in 2015, suggesting that the underlying dike was shallower, on average just 10 m below the surface, but similar in width. These two grabens, at 1.3–1.7 km in length, are longer than others mapped on the Juan de Fuca Ridge

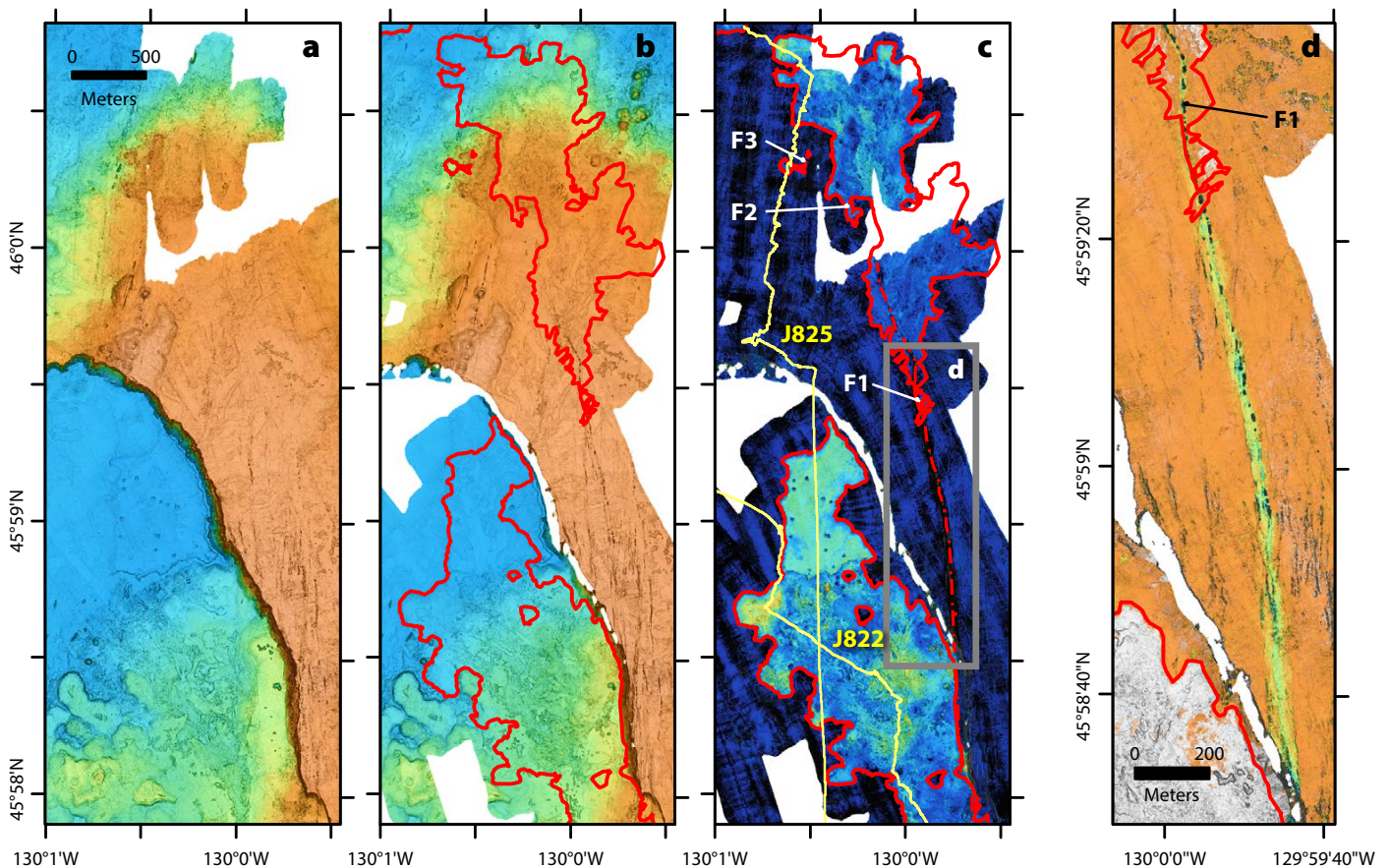


FIGURE 7. Flows, fissures, and a graben that resulted from the 2015 eruption on the east to northeast rim of the caldera. (a) Pre-eruption AUV bathymetry, and (b) post-eruption AUV bathymetry. Color ramp for (a) and (b) is 1,823–1,367 m depth (blue to orange). (c) Difference map from AUV bathymetry showing flows on caldera floor to the southwest and flows on the northeast rim. Color ramp is 0–15 m thickness (blue to orange) (d) Close-up of a graben formed by a dike injection that also produced a discontinuous open fissure. Color ramp is –4 to +1 m thickness (blue to orange). (a, b, c) are at a uniform scale. Location of (d) is shown by the gray box in (c). Flow outlines were determined from difference with ship data where pre-eruption AUV coverage was lacking. ROV *Jason* dives J822 and J825 are indicated by yellow lines in (c). Flow outlines as in Figure 1, and fissures for the 2015 eruption are marked with dashed lines.

(Chadwick and Embley, 1998).

Fragmented lava pillows are common in the 2015 flows (Figure 10a) and are thought to be the cause of abundant explosive sounds recorded during the eruption (Chadwick et al., 2016; Wilcock et al., 2016). During roughly 45 ROV dives by MBARI on Axial Seamount in the past 10 years, fragmented pillows were observed only rarely. These fragmented flows are distinct from collapsed lobate flows in several ways. First, they generally form in pillow instead of lobate lavas. Second, some fragments of the pillow are ejected outside the main fragmented area. Third, the lava fragments tend to be extensively broken into small pieces (most <5 cm across) of mainly non-glassy lava. Such fragmented pillows in the 1998 lava flows were observed in active hydrothermal areas with tubeworm clumps and orange-brown hydrothermal staining. The 2011 flows have rare fragmented pillows around the pillow margins of the flow on the east rim of the caldera where the flows buried 1–2 m thick sediment. The 2011 lava flow burrowed under some sediment, creating a lumpy sediment surface texture with a darkened color (Figure 6b). Fragmented pillows have also been observed in pre-historic flows at Axial Seamount, but only rarely. In contrast, the 2015 flows have many thousands of fragmented pillows (Chadwick et al., 2016), an observation confirmed during 2016 ROV dives. The physical setting of many of the fragmented pillows near flow margins or near sites of low-temperature hydrothermal venting, combined with the non-glassy character of the fragments produced, support the idea that these are formed by steam explosions under solid lava flows rather than being driven by release of magmatic gases or by collapse when molten lava drained.

Continuing northward on the north rift, the pre-eruption bathymetry is ship-based. Narrow fissures and thin parts of flows were not resolved (Figure 8b) until AUV mapping revealed flow margins and the ROV observations found the lavas to

appear fresh and still cooling. North of the two thin channelized flows, a wide fissure marks the path of the dike for ~1.7 km (F1 on Figure 8b) but remains unexplored. North of that, the fissure was filled with lava that spilled out only to the east at the southern end and to the east and west farther north (Figure 8b). The lava drained out of the fissure, leaving drapery-folded lava coatings and thin jumbled sheet flows. A deep non-eruptive fissure (F2 on Figure 8) continued another 1.7 km to the north before lava again overflowed and fed a small thin

channelized flow that extends ~200 m to the northeast. The fissure steps west again at this point. Low-temperature vents characterized by white microbial mats (Figure 10c) are common within the fissure and on adjacent flows; some have more diverse vent communities, including occasional clusters of small *Ridgeia* tubeworms and scale worms that were observed in August 2016.

The northernmost area of the 2015 flow starts with ~900 m of non-eruptive fissure (F1 on Figure 9a) that erupted channelized flows on both sides of the

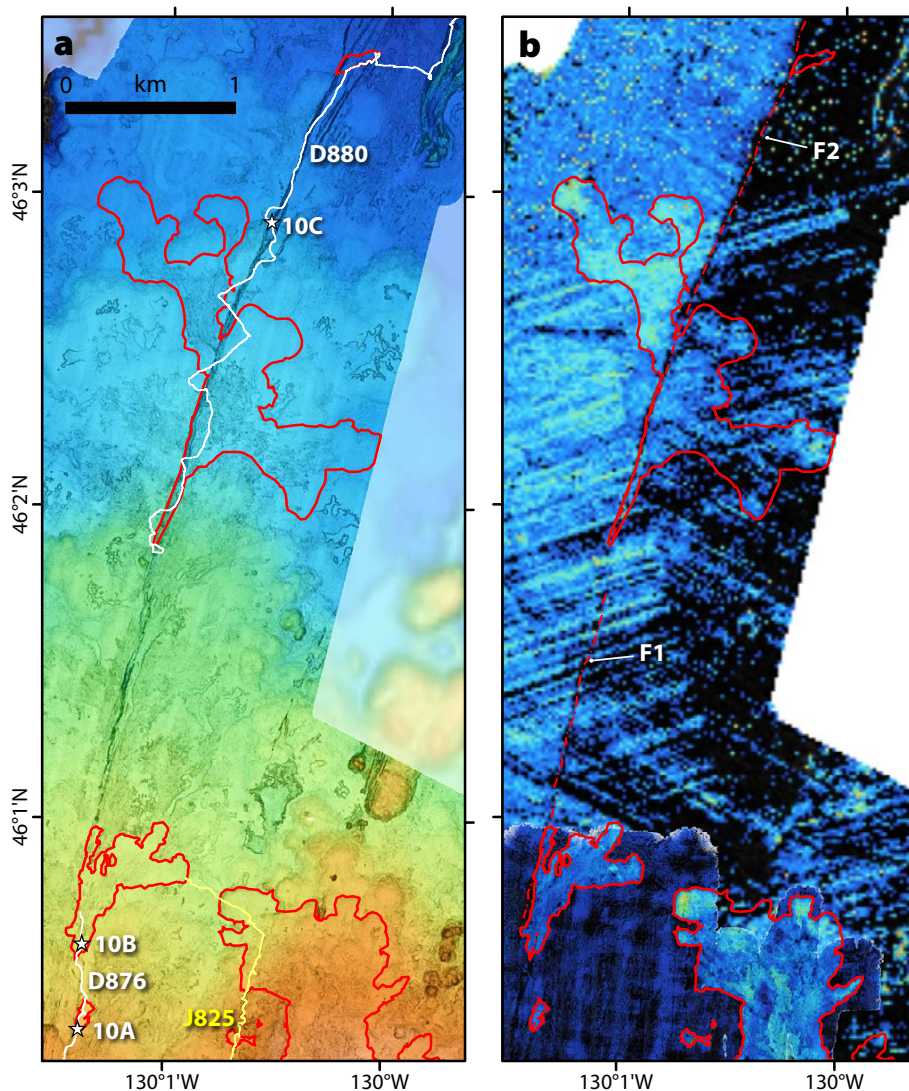


FIGURE 8. (a) Upper north rift showing 2015 lava flows and fissures on post-eruption AUV data superposed on ship bathymetry at 25 m resolution. Color ramp is 1,700–1,475 m depth (blue to orange). Lava flow boundaries and fissures as in Figure 1. ROV *Doc Ricketts* dives D876 and D880 are shown as white lines and ROV *Jason* dive J825 as a yellow line. Stars indicate locations of bottom photographs in Figure 10. (b) Difference map between post-eruption AUV data and either pre-eruption ship data (northern section) or AUV data (southern section). Flow outline and fissure as in Figure 1. Color ramp is 0–15 m. The difference map shows vertical offset across the north rift fissure with the west side uplifted relative to the east side.

fissure at its northern end. The fissure changes trend from N14E at the southern end to N22E at the northern end. This next 1.5 km of fissure erupted channelized flows with open sheet flow channels and distal inflated pillow margins. A small conical hummocky flow about 300 m across is centered on the eruptive fissure (HF on Figure 9b), atop the channelized flow. A hummocky flow on top of an earlier channelized flow is evidence that the eruption rate decreased during the eruption, as has been observed in

terrestrial volcanoes (e.g., Mauna Loa in 1984; Lockwood et al., 1987). The hummocky flow in Figure 9b was built on top of the eruptive fissure and covered broad lava channels of the earlier channelized-flow phase of the eruption. This hummocky flow is nearly 6 km up-rift of the most distal flow.

Starting about 1.2 km to the north-northeast of the small hummocky flow, the flows become largely hummocky. The northernmost of these is complex, with an intricate network

of subsurface tubes extending off axis (Le Saout et al., 2017; Figure 9c). Despite its complexity and the variety of tumuli and partly drained lava ponds on the summit of this roughly flat-topped feature, it is a hummocky flow.

The fissure system steps about 500 m to the northwest just north of the mound in Figure 9c, maintaining its N22E orientation. It erupted two adjacent hummocky flows with only a narrow gap between them. These show very subtle collapse features on the lobes that

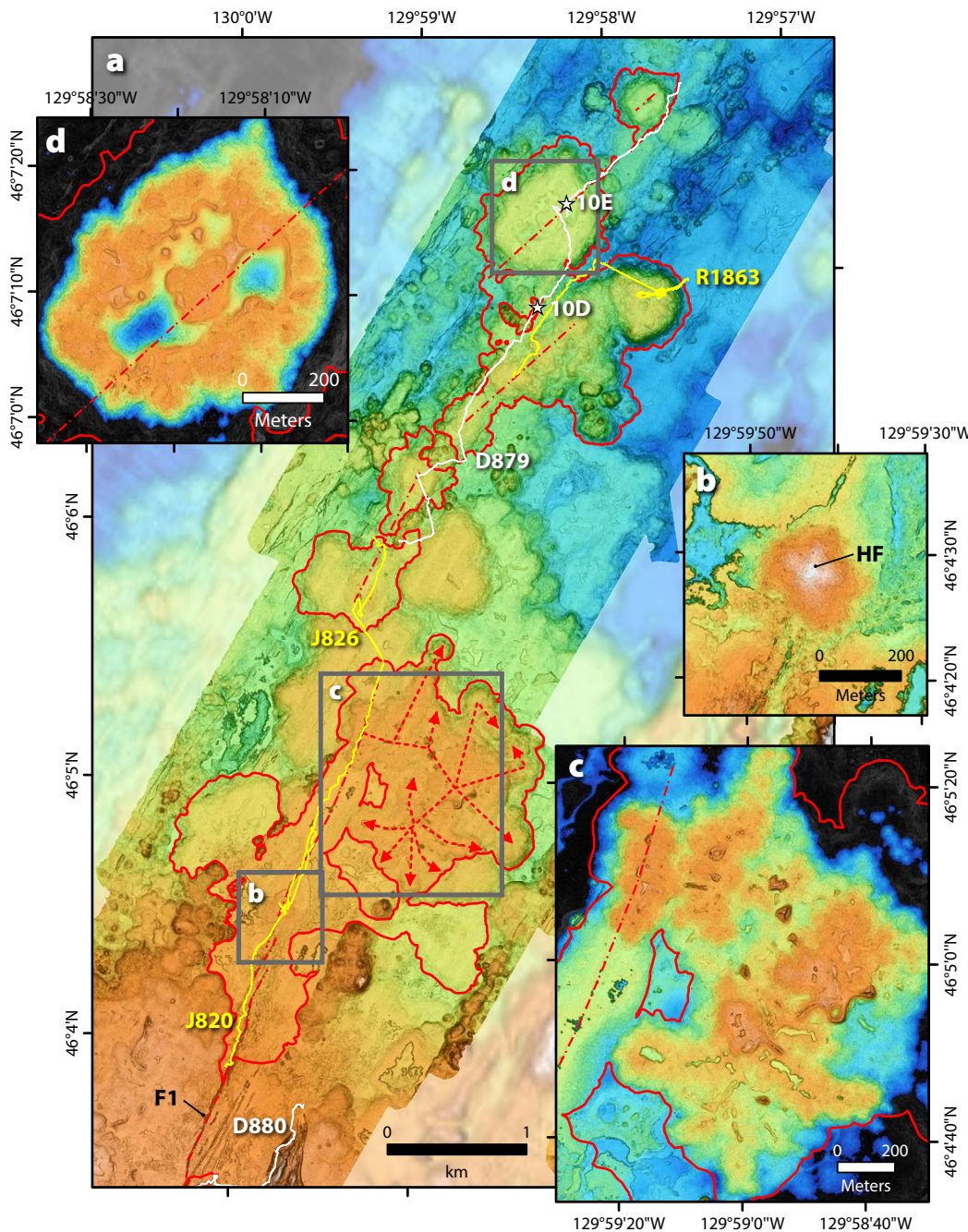


FIGURE 9. (a) Middle north rift showing 2015 lava flows and fissures on post-eruption AUV data superposed on ship-collected bathymetry at 25 m resolution. Locations of the close-ups of the pillow mound on top of inflated lobate flow (b), and inflated pillow mounds (c, d) are indicated by gray boxes in (a). Numerous tumuli and small lava lakes decorate the summit. Lava flow boundaries are indicated as in Figure 2, and fissures are shown as color-matched dashed lines. Color ramp is 1,900–1,650 m depth (blue to orange). (b) A low pillow mound constructed on top of inflated lobate flows indicates that eruption rates decreased as the eruption proceeded. Color ramp is 1,762–1,755 m depth (blue to orange). (c) Summit of complex inflated pillow mounds mainly constructed adjacent to the eruptive fissure, with interpreted subsurface tube distribution system (Le Saout et al., 2017). (d) Summit platform of inflated pillow mound perched on an eruptive fissure exhibits lava lakes with levees and depressed areas of drain-back. Color ramp is 1,740–1,715 m depth (blue to orange). (c) and (d) are at the same scale. ROV *Doc Ricketts* dives D879 and D880 are shown as white lines and ROV *Jason* dives J820 and J826 and ROPOS dive R1863 as yellow lines. Stars indicate locations of bottom photographs in Figure 10.

advanced away from the fissure and formed as lava drained from the molten flow interior. The three northernmost fissures (with that in Figure 9d being the middle one) are oriented N47E, offset from one another to the north by 650 m and then by another 200 m. The orientation of these three 2015 fissures parallels a series of older fissures that were not buried by the 2015 flows and are located east of Figure 9d and ~30° oblique to the trend of the north rift axis. The thickest of the northernmost 2015 hummocky

flows is 126 m thick (the mound that dive R1863 focused upon, Figure 9a).

Mounds produced from the fissure south of Figure 9d are hummocky flows lacking collapses. The distal pillowed margins of these flows drape into pre-existing open fissures (Figure 10d). In other places, 2015 lava is visible down in some open fissures, such as between the hummocky flow shown in Figure 9d and the adjacent hummocky flow to the northeast. The two northernmost mounds are hummocky flows

constructed atop the eruptive fissures instead of being distal flow lobes.

A complex lava pond lies on top of the nearly flat-topped 66 m thick hummocky flow in Figure 9d. The pond measures about 200 m × 400 m and is surrounded by low levees. The pond partly drained, creating the depressions. Numerous tiny (~10–30 cm tall) active black smoker chimneys (Figure 10e,f) were observed in August 2016 and again in August 2017 on the summit of this mound along with extensive bacterial mats and occasional

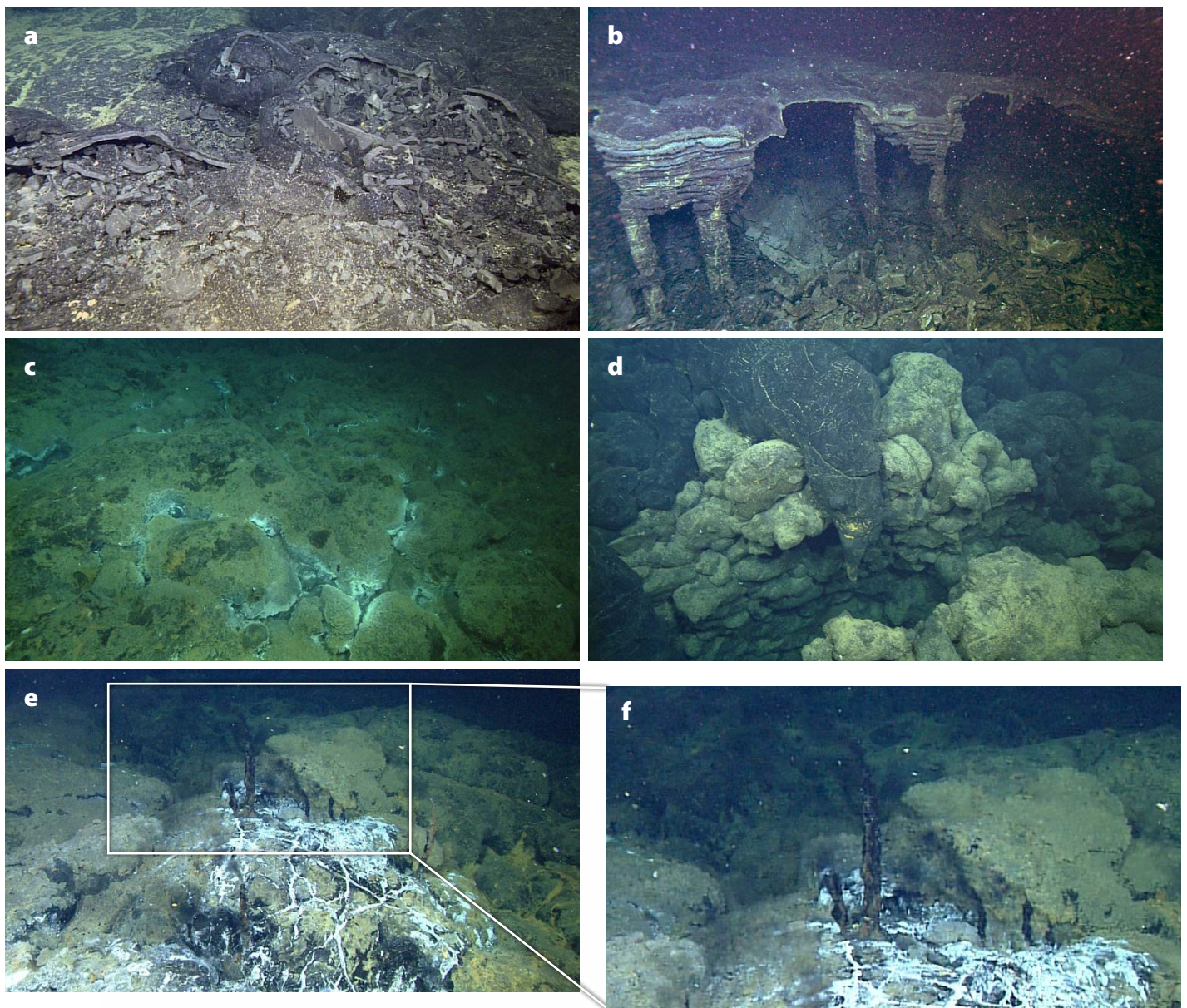


FIGURE 10. Plate of bottom photos of 2015 flow from ROV *Doc Ricketts*, with locations shown on Figures 8 and 9. (a) Fragmented pillows in 2015 north rift flow. (b) 2015 upper north rift lava lake and skinny pillars ~2–4 m tall. (c) 2015 fissure on upper north rift with extensive orange hydrothermal deposits. (d) 2015 flow on north rift flowing into open fissure in older lava. (e) Thick hummocky flow with active black smoker chimneys from lower north rift. (f) Close-up of the chimneys in (e).

scale and *Paralvinella* worms. Chemical and microscopic analysis of the chimneys shows them to be composed almost entirely of Fe-sulfides and anhydrite with very low abundances of Cu, Zn, Pb, or metals other than Fe. These northernmost 2015 hummocky flows reach up to 126 m thick, and others ranged between 35 m and 73 m thick. The two complex mounds illustrated in Figure 9c,d are 59 m and 66 m thick, respectively. Areas, volumes,

lava ponds on their upper, near-flat surfaces. Many hummocky flows of a range of sizes are located adjacent to inferred fissures that fed lava to them. One of these flows (Figure 9c) has a volume of $38.6 \times 10^6 \text{ m}^3$ and was apparently active for the entire 28-day eruption, based on acoustic records of explosion sounds (Wilcock et al., 2016; Caplan-Auerbach et al., 2017). Likewise, another complex hummocky flow (Figure 9d) has a vol-

ume of $21.3 \times 10^6 \text{ m}^3$ and erupted for at least 12 days, again based on the timing of recorded explosive noises. Lava was fed through a maze of lava tubes within the hummocky flow, as indicated by locations of the explosions and the morphology of the surface (red dashed lines in Figure 9; Le Saout et al., 2017). If activity lasts longer than that of the 2015 Axial eruption, complex hummocky flows (Figure 9c,d) may grow to become small flat-topped seamounts, like Cage Seamount (with a volume of $\sim 121 \times 10^6 \text{ m}^3$; Embley et al., 1995) located on the CoAxial segment of the Juan de Fuca Ridge adjacent to the 1993 hummocky flows.

ERUPTION DURATION AND RATES

Accurate flow volumes and eruption durations are required to determine average eruption rates. Eruption rates probably start out high and decrease through an eruption, as illustrated in Figure 9b, where a mound of hummocky flow erupted after channelized flows. Average eruption rates might therefore be substantially lower than maximum eruption rates that probably occurred during the initial phase of each eruption. The repeat AUV mapping provides accurate volumes for flows and flow lobes, and difference maps using ship-based bathymetry are sufficiently accurate for thick hummocky flows, but less reliable for thinner channelized flows. Eruption durations, on the other hand, are less well constrained.

For example, the 1998 eruption was estimated to have taken 11 days based on the duration of the associated seismic swarm (Dziak and Fox, 1999). This yields an average eruption rate of just $25 \text{ m}^3 \text{ s}^{-1}$, which is in the range expected for hummocky flows (Griffiths and Fink, 1992; Gregg and Fink, 1995), yet these were exclusively channelized flows. Eruption rates more in line with expectations for a channelized flow are at least an order of magnitude greater. If the eruption ended either when the earthquake swarm migrated down-rift past the eruptive fissure (9:24 hr:min from the time of the initial earthquake swarm) or when it reached the distal south end of the rift (22:27; Dziak and Fox, 1999), then the average eruption rates would be $712 \text{ m}^3 \text{ s}^{-1}$ and $292 \text{ m}^3 \text{ s}^{-1}$, respectively. The higher rate is similar to that estimated by Chadwick et al. (2013) using a duration to produce the northern, largest channelized flow of 12 hours. The 22:27 duration and $292 \text{ m}^3 \text{ s}^{-1}$ rate are

“ If the past is the key to the future, then future eruptions at Axial Seamount will likely begin with eruption of $\sim 25 \times 10^6 \text{ m}^3$ of fluid channelized flows in and near the caldera. ”

and inferred fissure lengths are summarized in Table 1. Elsewhere along the 2015 fissure on the north rift, low-temperature venting supported abundant bacterial mats and occasional vent megafauna, and deposited abundant orange-brown hydrothermal mat 16 months after the eruption. The discovery of venting here and in the 2011 hummocky flows on the south rift shows that the cooling of thick hummocky flows takes more than three years, and extraction of heat from cooling dikes beneath fissures drives low-temperature hydrothermal circulation that continues for multiple years. In the event that a thick hummocky flow is constructed on top of the dike, it may generate a high-temperature hydrothermal system, and sulfide chimneys may still grow there more than 28 months after the eruption.

The AUV mapping shows that the 2015 hummocky flows on the middle north rift (Figure 9c,d) are the most complex hummocky flows formed during the three eruptions at Axial Seamount; they exhibited large volumes of molten material not only in their cores but also as

The new mapping data unequivocally show that hummocky flows do not consist solely of constructional piles of pillows, as depicted in Figure 2 of Chadwick et al. (2013), as they must also have molten cores that can drain and lead to surface collapse, depending on the thickness of the solid crust and connectivity that allows molten lava to drain from the interior. These molten interiors allow construction of hummocky flows adjacent

reasonable for the average eruption rate of all the 1998 channelized flows and suggests that the eruption most likely ended as the dike advanced to the distal end of the south rift. For comparison, the fissure eruption on Mauna Loa in 1984 had an eruption rate of between $280 \text{ m}^3 \text{ s}^{-1}$ and $560 \text{ m}^3 \text{ s}^{-1}$ ($1\text{--}2 \times 10^6 \text{ m}^3 \text{ hr}^{-1}$) during the initial stages of the eruption (Lockwood et al., 1987), whereas Kilauea's high-fountain phases early in the current eruption ranged from $17\text{--}367 \text{ m}^3 \text{ s}^{-1}$ (Parfitt et al., 1995).

The similarity in volume and morphology of the summit and near-summit channelized flows produced in 2011 and 1998 suggest that they erupted for similar durations and at similar rates. The 1998 and 2015 channelized flows have narrow lobate margins and extensive channel systems compared with the wide lobate margins and narrow channel systems of the 2011 flows, presumably indicating somewhat different eruption rates even for the channelized flow portions of the eruptions. The channelized flows in the summit and upper rift zones from all three eruptions likely erupted in less than 24 hours.

On the other hand, the entire 2011 eruption was estimated to have lasted six days (Chadwick et al., 2012) based on the duration of deflation at the summit, after which it began to re-inflate. The eruption rate that formed the lower rift pillow ridge can be evaluated, assuming the dike took a day to propagate down the south rift zone, as it did in 1998 (Dziak and Fox, 1999). This five-day eruption duration yields an average eruption rate of $\sim 140 \text{ m}^3 \text{ s}^{-1}$. However, the steep hummocky flow (Figure 5, pillow ridge B of Caress et al., 2012) has the morphology expected for very low eruption rates (e.g., $<1 \text{ m}^3 \text{ s}^{-1}$; Griffiths and Fink, 1992; Gregg and Fink, 1995). Based on feasible, but perhaps still too high, eruption rates of $23 \text{ m}^3 \text{ s}^{-1}$ and $17 \text{ m}^3 \text{ s}^{-1}$, we calculate eruption durations of 30 and 40 days. The low expected eruption rates suggest that the 2011 eruption lasted at least a month, and that summit re-inflation commenced

before the eruption on the lower south rift ended. Dziak et al. (2012) showed that volcanic tremor continued at least until April 19, or 13 days after the start of the eruption, supporting a longer inferred eruption duration.

The detection and locations of explosive sounds during the 2015 eruption (Wilcock et al., 2016; Caplan-Auerbach et al., 2017) provide a new observation to constrain the duration of an eruption and cooling of flows. The period of intense explosive noises located within the caldera and on its northeast rim was limited to about 1.5 days after the eruption began. If all the channelized flows erupted during this 1.5-day period, the eruption rate would be about $190 \text{ m}^3 \text{ s}^{-1}$, which is consistent with the expected rate for this flow morphology (Griffiths and Fink, 1992; Gregg and Fink, 1995).

The explosive sounds lasted longer on the middle north rift zone, suggesting the entire group of complex hummocky flows, with a volume of $130.5 \times 10^6 \text{ m}^3$, erupted in no more than the 27-day duration of the sounds, for an overall average eruption rate of $56 \text{ m}^3 \text{ s}^{-1}$. The eruption durations of individual 2015 hummocky flows (Figure 9c,d) can also be constrained by the distribution in time of explosive sounds (Wilcock et al., 2016; Caplan-Auerbach et al., 2017). The hummocky flow in Figure 9c has a volume of $38.6 \times 10^6 \text{ m}^3$, and explosions were recorded there for the entire eruption. These values yield an average eruption rate of $16 \text{ m}^3 \text{ s}^{-1}$ for this flow alone. The hummocky flow in Figure 9d has a volume of $21.3 \times 10^6 \text{ m}^3$, and explosions were located there for the first seven days of the eruption. These values yield an average eruption rate of $35 \text{ m}^3 \text{ s}^{-1}$ to form this flow alone.

The estimated average eruption rates for the 2015 channelized flows of $190 \text{ m}^3 \text{ s}^{-1}$ and for the hummocky flows of $<56 \text{ m}^3 \text{ s}^{-1}$ are consistent with higher eruption rates for thin channelized flows than for thicker hummocky flows, as proposed by Griffiths and Fink (1992) and Gregg and Fink (1995), but would also

support eruption rates to form the lower rift 2011 hummocky flow significantly less than $16\text{--}35 \text{ m}^3 \text{ s}^{-1}$. These values suggest that the eruption rate for the 2011 lower south rift hummocky flow should be lower still, with the eruption lasting even longer than 40 days.

These estimated average eruption rates suggest that the 1998 eruption was much shorter in duration than the accompanying earthquake swarm and that the 2011 eruption lasted far beyond the end of summit deflation. These discrepancies highlight the need to improve determination of durations of eruptive activity when visual observations are lacking. The explosive sounds recorded in 2015 might be just such a tool, although fragmented lavas are far more abundant in the 2015 flows than the 2011, 1998, or other prehistoric flows, so if the explosive sounds are associated with formation of the fragmented pillows, explosions may be far less common in future eruptions than in 2015.

WHAT'S NEXT?

The channelized flow portions of all three eruptions have similar areas ($6.92\text{--}8.24 \times 10^6 \text{ m}^2$) and volumes ($24.1\text{--}28.7 \times 10^6 \text{ m}^3$) (see Table 1). The 1998, 2011, and 2015 eruptions produced channelized flows from similar distances of the uppermost fissures for 11 km, 12.7 km (includes non-eruptive fissures at each end), and 15 km, respectively. Their eruption volumes per km of active eruptive fissure are also similar, ranging from $3.0\text{--}3.5 \times 10^6 \text{ m}^3 \text{ km}^{-1}$ of fissure (with the 1988 flows exhibiting the lowest volume per kilometer of fissure). If the past is the key to the future, then future eruptions at Axial Seamount will likely begin with eruption of $\sim 25 \times 10^6 \text{ m}^3$ of fluid channelized flows in and near the caldera. The large differences in total volumes of the three eruptions are due to differences in the production of thick hummocky flows down the rift zones, and such flows may or may not follow the eruption of near-summit channelized flows.

CONCLUSIONS

1. AUVs equipped with multibeam sonars can produce meter-scale bathymetric maps, following data processing to reduce navigational offsets to the same order. MBARI played a crucial role in the development of mapping AUVs and the data processing required to produce high-resolution maps that illuminate lava flow types and their emplacement dynamics.
2. The 1998, 2011, and 2015 eruptions at Axial Seamount produced morphologically similar channelized flows inside and near the caldera. Each covered areas of ~7–8 km² and erupted lava volumes of ~25 × 10⁶ m³.
3. The 2011 and 2015 eruptions also produced hummocky flows consisting largely of pillow lava in the upper to middle rifts, in both cases with channelized flows immediately up-rift from the shallowest hummocky flows.
4. The 2011 eruption was the only one that also produced a steep hummocky flow on the lower south rift, which was separated from the upper rift hummocky flows by an 18 km-long non-eruptive gap.
5. Hummocky flows that have molten cores can be identified by off-fissure growth of lava flows fed from on-fissure mounds, collapse pits in their summits, or in the 2015 examples, by complex levee-enclosed lava ponds and tumuli on their surfaces. Hummocky flows can form above eruptive fissures or adjacent to fissures. These characteristics change as eruption rate changes.
6. Eruption rates of channelized flows are greater than those of hummocky flows with large molten cores, which are greater than those of hummocky flows with small molten cores.
7. Methods used to determine the duration of activity that produced the various lava flows or parts of lava flows are typically less accurate than the determination of eruptive volumes. The 1998 eruption probably lasted no more than a few days instead of the

12 days inferred from seismicity, and the 2011 eruption likely lasted longer than a month instead of the six days inferred from the duration of deflation at the summit. The acoustic signals recorded in 2015 may be the most reliable measure of continuing eruptive activity, although explosions may continue during a short period of flow cooling beyond the end of the eruption, and not all eruptions may produce such abundant explosive noises as the 2015 eruption.

8. Future eruptions are likely to consist of summit and upper-rift eruptions of channelized flows similar in volume and area covered to those erupted in 1998, 2011, and 2015 and may also form hummocky flows along the upper to lower rifts, regardless of whether the eruption propagates down the north or south rift. ☒

REFERENCES

- Arnulf, A.F., A.J. Harding, G.M. Kent, S.M. Carbotte, J.P. Canales, and M.R. Nedimovic. 2014. Anatomy of an active submarine volcano. *Geology* 42(8):655–658, <https://doi.org/10.1130/G356291>.
- Baker, E.T., C.G. Fox and J.P. Cowen. 1999. In situ observations of the onset of hydrothermal discharge during the 1998 submarine eruption of Axial Volcano, Juan de Fuca Ridge. *Geophysical Research Letters* 26(23):3,445–3,448, <https://doi.org/10.1029/1999GL002331>.
- Ballard, R.D., R.T. Holcomb, and T.H. van Andel. 1979. The Galapagos rift at 86°W: Part 3. Sheet flows, collapse pits, and lava lakes of the rift valley. *Journal of Geophysical Research* 84:5,407–5,422, <https://doi.org/10.1029/JB084iB10p05407>.
- Ballard, R.D., and T.H. van Andel. 1977. Morphology and tectonics of the inner rift valley at 36°50'N on the Mid-Atlantic Ridge. *Geological Society of America Bulletin* 88:507–530.
- Caplan-Auerbach, J., R.P. Dziak, J. Haxel, R.R. Bohnenstiehl, and C. Garcia. 2017. Explosive processes during the 2015 eruption at Axial Seamount, as recorded by seafloor hydrophones. *Geochemistry, Geophysics, Geosystems* 18:1,761–1,774, <https://doi.org/10.1002/2016GC006734>.
- Caress, D.W., and D.N. Chayes. 2011. MB-System: Mapping the Seafloor, <http://www.mbari.org/data/mbsystem>, open source software distributed from the MBARI and LDEO websites.
- Caress, D.W., and D.N. Chayes. 1996. Improved processing of Hydrosweep DS multibeam data on the R/V *Maurice Ewing*. *Marine Geophysical Researches* 18:631–650, <https://doi.org/10.1007/BF00313878>.
- Caress, D.W., D.A. Clague, J.B. Paduan, J. Martin, B. Dreyer, W.W. Chadwick Jr., A. Denny, and D.S. Kelley. 2012. Repeat bathymetric surveys at 1-metre resolution of lava flows erupted at Axial Seamount in April 2011. *Nature Geoscience* 5(7):483–488, <https://doi.org/10.1038/NNGEO1496>.
- Caress, D.W., D.A. Clague, J.B. Paduan, and H. Thomas. 2015. Vertical deformation of the Axial Seamount summit from repeated 1-m scale bathymetric surveys with the MBARI mapping AUV. *Geological Society of America Annual Meeting, Baltimore, Maryland, November 1–4, 2015, Abstracts with Programs* 47(7):381.
- Caress, D.W., D.A. Clague, J.B. Paduan, H.J. Thomas, W.W. Chadwick, S.L. Nooner, and D. Yoerger. 2016. Vertical deformation of the Axial Seamount summit from repeated 1-m scale bathymetry surveys using AUVs. *American Geophysical Union Fall Meeting, San Francisco, December 12–16, 2016, Abstract OS41C-1991*.
- Caress, D.W., H. Thomas, W.J. Kirkwood, R. McEwen, R. Henthorn, D.A. Clague, C.K. Paull, J. Paduan, and K.L. Maier. 2008. High-resolution multibeam, sidescan, and subbottom surveys using the MBARI AUV *D. Allan B*. Pp. 47–69 in *Marine Habitat Mapping Technology for Alaska*. J.R. Reynolds and H.G. Greene, eds, Alaska Sea Grant College Program, University of Alaska Fairbanks, <https://doi.org/10.4027/mhmta.2008.04>.
- Chadwick, W.W. Jr., D.A. Clague, R.W. Embley, M.R. Perfit, D.A. Butterfield. D.W. Caress, J.B. Paduan, J.F. Martin, P. Sasnett, S.G. Merle, and A.M. Bobbitt. 2013. The 1998 eruption of Axial Seamount: New insights on submarine lava flow emplacement from high-resolution mapping. *Geochemistry, Geophysics, Geosystems* 14:3,939–3,968, <https://doi.org/10.1002/ggge.20202>.
- Chadwick, W.W. Jr., and R.W. Embley. 1998. Graben formation associated with recent dike intrusions and volcanic eruptions on the mid-ocean ridge. *Journal of Geophysical Research* 103(B5):9,807–9,825, <https://doi.org/10.1029/97JB02485>.
- Chadwick, W.W. Jr., R.W. Embley, and C.G. Fox. 1991. Evidence for volcanic eruption on the southern Juan de Fuca Ridge between 1981 and 1987. *Nature* 350:416–418, <https://doi.org/10.1038/350416a0>.
- Chadwick, W.W. Jr., R.W. Embley, and T.M. Shank. 1998. The 1996 Gorda Ridge eruption: Geologic mapping, sidescan sonar, and SeaBeam comparison results. *Deep Sea Research Part II* 45:2,547–2,569, [https://doi.org/10.1016/S0967-0645\(98\)00083-6](https://doi.org/10.1016/S0967-0645(98)00083-6).
- Chadwick, W.W. Jr., S.L. Nooner, D.A. Butterfield, and M.D. Lilley. 2012. Seafloor deformation and forecasts of the April 2011 eruption at Axial Seamount. *Nature Geoscience* 5(7):474–477, <https://doi.org/10.1038/NNGEO1464>.
- Chadwick, W.W. Jr., J.B. Paduan, D.A. Clague, B.M. Dreyer, S.G. Merle, A.M. Bobbitt, D.W. Caress, B.T. Philip, D.S. Kelley, and S.L. Nooner. 2016. Voluminous eruption from a zoned magma body after an increase in supply rate at Axial Seamount. *Geophysical Research Letters* 43:12,063–12,070, <https://doi.org/10.1002/2016GL071327>.
- Chadwick, W.W. Jr., D.S. Scheirer, R.W. Embley, and H.P. Johnson. 2001. High-resolution bathymetric surveys using scanning sonars: Lava flow morphology, hydrothermal vents, and geologic structure at recent eruption sites on the Juan de Fuca Ridge. *Journal of Geophysical Research* 106:16,075–16,099, <https://doi.org/10.1029/2001JB000297>.
- Clague, D.A., B.M. Dreyer, J.B. Paduan, J.F. Martin, D.W. Caress, J.B. Gill, D.S. Kelley, H. Thomas, R.A. Portner, T.P. Guilderson, and M.L. McGann. 2014. Eruptive and tectonic history of the Endeavour segment of the Juan de Fuca Ridge based on AUV mapping and lava flow ages. *Geochemistry, Geophysics, Geosystems* 15:1–28, <https://doi.org/10.1002/2014GC005415>.
- Clague, D.A., W.W. Chadwick Jr., A.S. Davis, J.W. Head III, L.G. Mastin, J.B. Paduan, S.L. Ross, L. Wilson, and R.A. Zierenberg. 2005. A new

- look at the 1996 Gorda Ridge eruption. American Geophysical Union 2005 Fall Meeting Supplement, Abstract T4E-1360.
- Clague, D.A., A.S. Davis, and J.E. Dixon. 2003. Submarine strombolian eruptions on the Gorda mid-ocean ridge. In *Explosive Subaqueous Volcanism*. Geophysical Monograph Series, vol. 140, American Geophysical Union, Washington, DC, <https://doi.org/10.1029/140GM07>.
- Clague, D.A., B.M. Dreyer, J.B. Paduan, J.F. Martin, W.W. Chadwick Jr., D.W. Caress, R.A. Portner, T.P. Guilderson, M.L. McGann, D.A. Butterfield, and others. 2013. Geologic history of the summit of Axial Seamount, Juan de Fuca Ridge. *Geochemistry, Geophysics, Geosystems* 14:4,403–4,443, <https://doi.org/10.1002/ggge.20240>.
- Crisp, J.A. 1984. Rates of magma emplacement and volcanic output. *Journal of Volcanology and Geothermal Research* 20:177–211, [https://doi.org/10.1016/0377-0273\(84\)90039-8](https://doi.org/10.1016/0377-0273(84)90039-8).
- Dreyer, B.M., D.A. Clague, and J.B. Gill. 2013. Petrological variability of recent magmatism at Axial Seamount summit, Juan de Fuca Ridge. *Geochemistry, Geophysics, Geosystems* 14(10):4,306–4,333, <https://doi.org/10.1002/ggge.20239>.
- Dziak, R.P., and C.G. Fox. 1999. The January 1998 earthquake swarm at Axial Volcano, Juan de Fuca Ridge: Hydroacoustic evidence of sea-floor volcanic activity. *Geophysical Research Letters* 26(23):3,429–3,432, <https://doi.org/10.1029/1999GL002332>.
- Dziak, R.P., J.H. Haxel, D. Bohnenstiehl, and H. Matsumoto. 2012. Seismic precursors and magma ascent before the April 2011 eruption at Axial Seamount. *Nature Geoscience* 5:478–482, <https://doi.org/10.1038/ngeo1490>.
- Embley, R.W., and E.T. Baker. 1999. Interdisciplinary group explores seafloor eruption with remotely operated vehicle. *Eos, Transactions of the American Geophysical Union* 80(19):213–222, <https://doi.org/10.1029/99EO00157>.
- Embley, R.W., W.W. Chadwick Jr., D. Clague, and D. Stakes. 1999. The 1998 eruption of Axial Volcano: Multibeam anomalies and seafloor observations. *Geophysical Research Letters* 26(23):3,425–2,428, <https://doi.org/10.1029/1999GL002328>.
- Embley, R.W., W.W. Chadwick Jr., I.R. Jonasson, D.A. Butterfield, and E.T. Baker. 1995. Initial results of the rapid response to the 1993 CoAxial event: Relationships between hydrothermal and volcanic processes. *Geophysical Research Letters* 22:143–146, <https://doi.org/10.1029/94GL02281>.
- Embley, R.W., W.W. Chadwick Jr., M.R. Perfit, M.C. Smith, and J.R. Delaney. 2000. Recent eruptions on the CoAxial segment of the Juan de Fuca Ridge: Implications for mid-ocean ridge accretion processes. *Journal of Geophysical Research* 105:16,501–16,525, <https://doi.org/10.1029/2000JB900030>.
- Fornari, D.J., K.L. Von Damm, J.G. Bryce, J.P. Cowen, V. Ferrini, A. Fundis, M.D. Lilley, G.W. Luther III, L.S. Mullineaux, M.R. Perfit, and others. 2012. The East Pacific Rise between 9°N and 10°N: Twenty-five years of integrated, multidisciplinary oceanic spreading center studies. *Oceanography* 25(1):18–43, <https://doi.org/10.5670/oceanog.2012.02>.
- Fox, C.G. 1999. In situ ground deformation measurements from the summit of Axial Volcano during the 1998 volcanic episode. *Geophysical Research Letters* 26(23):3,437–3,440, <https://doi.org/10.1029/1999GL900491>.
- Fox, C.G., W.W. Chadwick Jr., and R.W. Embley. 1992. Detection of changes in ridge-crest morphology using repeated multibeam surveys. *Journal of Geophysical Research* 97:11,149–11,162, <https://doi.org/10.1029/92JB00601>.
- Fox, C.G., W.W. Chadwick, Jr., and R.W. Embley. 2001. Direct observation of a submarine volcanic eruption from a sea-floor instrument caught in a lava flow. *Nature* 412:727–729, <https://doi.org/10.1038/35089066>.
- Gregg, T.K.P., and J.H. Fink. 1995. Quantification of submarine lava-flow morphology through analog experiments. *Geology* 23(1):73–76, [https://doi.org/10.1130/0091-7613\(1995\)023<0073:QOSLFM>2.3.CO;2](https://doi.org/10.1130/0091-7613(1995)023<0073:QOSLFM>2.3.CO;2).
- Griffiths, R.W., and J.H. Fink. 1992. Solidification and morphology of submarine lavas: A dependence on extrusion rate. *Journal of Geophysical Research* 97:19,729–19,737, <https://doi.org/10.1029/92JB01594>.
- Helo, C., M.-A. Longpré, N. Shimizu, D.A. Clague, and J. Stix. 2011. Explosive eruptions at mid-ocean ridges driven by CO₂-rich magmas. *Nature Geoscience* 4:260–263, <https://doi.org/10.1038/ngeo1104>.
- Kelley, D.S., J.R. Delaney, W.W. Chadwick Jr., B. Philp, and S.G. Merle. 2015. Axial Seamount 2015 eruption: A 127-m thick, microbially covered lava flow. Paper presented at the fall Meeting of the American Geophysical Union, San Francisco, CA, December 14–18, 2005, Abstract OS41B-08.
- Kelley, D.S., J.R. Delaney, and S.K. Juniper. 2014. Establishing a new era of submarine volcanic observatories: Cabling Axial Seamount and the Endeavour Segment of the Juan de Fuca Ridge. *Marine Geology* 352:426–450, <https://doi.org/10.1016/j.margeo.2014.03.010>.
- Le Saout, M., D.A. Clague, and J.B. Paduan. 2017. Morphological variability of the top of large inflated pillow mounds: Indication about eruptive processes. Paper presented at the Chapman Conference on Submarine Volcanism, Hobart, Australia, January 30–February 3, 2017.
- Lockwood, J.P., J.J. Dvorak, T.T. English, R.Y. Koyanagi, A.T. Okamura, M.L. Summers, and W.R. Tanigawa. 1987. Mauna Loa 1974–1984: A decade of intrusive and extrusive activity. Pp. 537–570 in *Volcanism in Hawaii*. R.W. Decker, T.L. Wright, and P.H. Stauffer, eds, U.S. Geological Survey Professional Paper 1350.
- MBARI Mapping Team. 2001. Seamounts and Ridges Multibeam Survey, Monterey Bay Aquarium Research Institute Digital Data Series No. 7, 1-CD.
- Moore, J.G., D.A. Clague, R.T. Holcomb, P.W. Lipman, W.R. Normark, and M. Torresson. 1989. Prodigious submarine landslides on the Hawaiian Ridge. *Journal of Geophysical Research* 94:17,465–17,484, <https://doi.org/10.1029/JB094iB12p17465>.
- Nooner, S.L., and W.W. Chadwick Jr. 2009. Volcanic inflation measured in the caldera of Axial Seamount: Implications for magma supply and future eruptions. *Geochemistry, Geophysics, Geosystems* 10, Q02002, <https://doi.org/10.1029/2008GC002315>.
- Nooner, S.L., and W.W. Chadwick Jr. 2016. Inflation-predictable behavior and co-eruption deformation at Axial Seamount. *Science* 354:1,399–1,403, <https://doi.org/10.1126/science.aah4666>.
- Orr, T.R. 2011. Lava tube shatter rings and their correlation with lava flux increases at Kilauea Volcano, Hawaii. *Bulletin of Volcanology* 73:335–346, <https://doi.org/10.1007/s00445-010-0414-3>.
- Paduan, J.B., D.A. Clague, and D.W. Caress. 2014. Constructional talus: Formed during eruption, not by later tectonism. Paper presented at the Fall Meeting of the American Geophysical Union, San Francisco, CA, December 15–19, 2014, Abstract V31B-4742.
- Parfitt, E.A., L. Wilson, and C.A. Neal. 1995. Factors influencing the height of Hawaiian lava fountains: Implications for the use of fountain height as an indicator of magma gas content. *Bulletin of Volcanology* 57:440–450, <https://doi.org/10.1007/BF00300988>.
- Portner, R.A., D.A. Clague, B.D. Dreyer, C. Helo, J.F. Martin, and J.B. Paduan. 2015. Contrasting styles of deep-marine explosive eruptions revealed from Axial Seamount push core records. *Earth and Planetary Science Letters* 423:219–231, <https://doi.org/10.1016/j.epsl.2015.03.043>.
- Rubin, K.H., S.A. Soule, W.W. Chadwick Jr., D.J. Fornari, D.A. Clague, R.W. Embley, E.T. Baker, M.R. Perfit, D.W. Caress, and R.P. Dziak. 2012. Volcanic eruptions in the deep sea. *Oceanography* 25(1):142–157, <https://doi.org/10.5670/oceanog.2012.12>.
- Soule, S.A., D.J. Fornari, M.R. Perfit, M.A. Tivey, W.I. Ridley, and H. Schouten. 2005. Channelized lava flows at the East Pacific Rise crest 9°–10°N: The importance of off-axis lava transport in developing crustal architecture. *Geochemistry, Geophysics, Geosystems* 6, Q08005, <https://doi.org/10.1029/2005GC000912>.
- White, S.M., K.C. Macdonald, and R.M. Haymon. 2000. Basaltic lava domes, lava lakes, and volcanic segmentation of the southern East Pacific Rise. *Journal of Geophysical Research* 105(B10):23,519–23,536, <https://doi.org/10.1029/2000JB900248>.
- Wilcock, W.S.D., M. Tolstoy, F. Waldhauser, C. Garcia, Y.J. Tan, D.R. Bohnenstiehl, J. Caplan-Auerbach, R.P. Dziak, A.F. Arnulf, and M.E. Mann. 2016. Seismic constraints on caldera dynamics from the 2015 Axial Seamount eruption. *Science* 354:1,395–1,399, <https://doi.org/10.1126/science.aah5563>.
- Yeo, I.A., D.A. Clague, J.F. Martin, J.B. Paduan, and D.W. Caress. 2013. Pre-eruptive flow focusing in dikes feeding historic pillow ridges on the Juan de Fuca and Gorda Ridges. *Geochemistry, Geophysics, Geosystems* 14:3,586–3,599, <https://doi.org/10.1002/ggge.20210>.

ACKNOWLEDGMENTS

Any project as long and complex as our study of Axial Seamount requires dedicated, skillful support from many people at sea and on shore. We have had such support from personnel on MBARI's ships *R/V Western Flyer*, *R/V Zephyr*, and *R/V Rachel Carson*, from the MBARI ROV and AUV operations teams, and from the crews of *R/V Thomas Thompson* and *R/V Atlantis*. The project was funded by annual grants to MBARI from the David and Lucile Packard Foundation, with additional support from the National Science Foundation and National Oceanic and Atmospheric Administration. PMEL contribution number 4675.

AUTHORS

David A. Clague (clague@mbari.org) is Senior Scientist, **Jennifer B. Paduan** is Research Specialist, and **David W. Caress** is Senior Software Engineer, all at the Monterey Bay Aquarium Research Institute, Moss Landing, CA, USA. **William W. Chadwick Jr.** is Oceanographer, National Oceanic and Atmospheric Administration, Pacific Marine Environmental Laboratory, Newport, OR, USA. **Morgane Le Saout** is Postdoctoral Fellow, Monterey Bay Aquarium Research Institute, Moss Landing, CA, USA. **Brian M. Dreyer** is Associate Specialist, Earth and Planetary Science Department, University of California, Santa Cruz, CA, USA. **Ryan A. Portner** is Assistant Professor, Geology Department, San Jose State University, San Jose, CA, USA.

ARTICLE CITATION

Clague, D.A., J.B. Paduan, D.W. Caress, W.W. Chadwick Jr., M. Le Saout, B.M. Dreyer, and R.A. Portner. 2017. High-resolution AUV mapping and targeted ROV observations of three historic lava flows at Axial Seamount. *Oceanography* 30(4):82–99, <https://doi.org/10.5670/oceanog.2017.426>.